

Thermalization and spectral distortions of the cosmic background radiation

Wayne Hu

Department of Physics, University of California, Berkeley, California 94720

Joseph Silk

Departments of Astronomy and Physics and Center for Particle Astrophysics, University of California, Berkeley, California 94720

(Received 17 November 1992)

Thermalization under double Compton scattering, bremsstrahlung, and elastic Compton scattering of an early energy injection of photons to the cosmic background radiation is examined both analytically and numerically. We find that spectral distortions in the Wien region can include negative as well as positive chemical potential distortions. The former must be evaluated numerically, whereas for the latter we compare analytic and numerical solutions. Spectral distortions in the Rayleigh-Jeans region are fixed by the Wien distortions and by the baryon density $\Omega_B h^2$. Thus, the Rayleigh-Jeans region can potentially provide constraints to $\Omega_B h^2$ should spectral distortions be seen in the cosmic background radiation. From an analysis of the time evolution of chemical potential distortions and the observational constraints on such distortions, significant energy injection at $z_h \lesssim 5 \times 10^5 (\Omega_B h^2)^{-2/5}$ is ruled out in all but a very small class of injection scenarios.

PACS number(s): 98.70.Vc, 98.80.Cq, 98.80.Es, 98.80.Hw

I. INTRODUCTION

The epoch of thermalization of the cosmic microwave background is the earliest direct probe of the big bang. The study of anisotropies probes the fluctuations that gave rise to large-scale structure at a redshift $z \lesssim 1000$, whereas spectral distortions are generated at $z \lesssim 10^7$. The proximity to a perfect blackbody spectrum, no deviations being measured to a limit of $\delta I/I = 0.03\%$ near the blackbody peak [1], already guarantees that any departures from the canonical model of a homogeneous and isotropic Friedmann-Lemaître universe were small at the thermalization epoch. Nevertheless, input of energy may have occurred, due, for example, to exotic out-of-equilibrium particle decays, to injection of primordial turbulence associated with decaying density fluctuation modes, or to early phase transition relics such as unstable domain walls or strings. It is important to examine deviations from a blackbody spectrum so as to be able to search for possible signatures of such decays. There is always the possibility that an experimental determination of distortions from a blackbody spectrum will be confirmed: historically, there have been several false alarms and, even at present, the low-frequency measurements continue to show marginally significant evidence of distortion. Perhaps, not least, there is the intellectual challenge of understanding precisely how the blackbody spectrum arises, and one can only achieve this by studying its evolution with time. It is for these reasons that we have undertaken a thorough study of photon injection and thermalization in the early Universe.

Thermalization processes require nonconservation of the photon number. The relevant interactions for cosmology are bremsstrahlung and double Compton scattering. An excellent review by Danese and De Zotti [2] summarizes the role of the Kompaneets equation in studying the spectral evolution under elastic Compton

scattering, the dominant process in coupling electrons and photons at early epochs, and of bremsstrahlung in achieving thermalization. Lightman [3] first showed quantitatively that double Compton scattering was of considerable importance in leading to thermalization, and more extensive calculations were done by Danese and De Zotti [4]. Burigana and co-workers [5,6] studied the numerical evolution of the spectrum for a small class of distortions at low redshifts $z \simeq 10^5 - 10^3$ as did Fukugita and Kawasaki [7]. However, evolution during the thermalization epoch, $z \simeq 10^5 - 10^7$ has only been treated by approximating the effect of photon creation [5,6,8]. In this paper, we treat the thermalization process more precisely by numerically evolving the spectrum. Moreover, we consider a broader class of energy injection in which both the energy and the number of photons injected are left as free parameters. We find two new classes of distortions, with Wien tails resembling a Bose-Einstein spectrum with negative chemical potential, and discuss their evolution. Furthermore, in all cases, there exists a certain universality in the spectral distortions that may in the future provide an independent measurement of the baryon density of the Universe $\Omega_B h^2$.

In the interests of making this treatment comprehensive and self-contained, we provide the analytic framework necessary for understanding the numerical solutions. The kinetic equations and equilibrium solution are given in Sec. II. Thermalization time scales are derived in Sec. III. We focus on instantaneous injection of photons and derive the high-frequency spectrum in Sec. IV, the low-frequency spectrum in Sec. V, and the time evolution of the chemical potential in Sec. VI. A final section presents a comparison of models with observations.

II. KINETIC EQUATIONS AND EQUILIBRIUM SOLUTIONS

By far, the dominant interaction coupling photons and electrons before recombination is elastic Compton

scattering, $\gamma + e \rightarrow \gamma + e$. The kinetic equation governing elastic Compton scattering was first derived by Kompaneets [9] to be

$$\left(\frac{\partial n}{\partial t} \right)_K = n_e \sigma_T c \left[\frac{k T_e}{m_e c^2} \right] \frac{1}{x_e^2} \frac{\partial}{\partial x_e} \times \left[x_e^4 \left(\frac{\partial n}{\partial x_e} + n + n^2 \right) \right], \quad (1)$$

where $n(x_e, t)$ is the photon occupation number, n_e is the electron number density σ_T is the Thomson cross section, T_e is the electron temperature, and $x_e = h\nu/kT_e$ is the dimensionless photon frequency. Equation (1) is commonly referred to as the Kompaneets equation. Before recombination, the electrons stay tightly coupled to the radiation. The physical photon frequency and the electron temperature scale in the same manner during the expansion. Thus, aside from a small correction,

$$x_e \frac{\partial n}{\partial x_e} \frac{\partial}{\partial t} \left[\ln \frac{T_e}{T_0(1+z)} \right]$$

added to the right-hand side of Eq. (1), the Kompaneets equation remains unchanged by the expansion [10]. Here T_0 is the temperature of the cosmic background radiation today. For our purposes, this correction term is always negligible due to the tight coupling between photons and electrons [2].

It is convenient for cosmological applications to reexpress the Kompaneets equation as

$$\left(\frac{\partial n}{\partial t} \right)_K = \frac{1}{t_K} \frac{1}{x_e^2} \frac{\partial}{\partial x_e} \left[x_e^4 \left(\frac{\partial n}{\partial x_e} + n + n^2 \right) \right], \quad (2)$$

where

$$t_K = 9.81 \times 10^{27} (1 - Y_p/2)^{-1} (\Omega_B h^2)^{-1} \times \Theta_{2.7}^{-1} \left[\frac{T_e}{T} \right]^{-1} z^{-4} \text{ s}, \quad (3)$$

for a fully ionized plasma. Here $\Theta_{2.7} = T_0/2.7$ K and $h = H_0/100 \text{ km s}^{-1} \text{ Mpc}^{-1}$. The primordial mass fraction of helium Y_p enters into the equation since $n_e = (1 - Y_p/2)n_B$ for a H+He plasma with n_B the number density of baryons. For numerical purposes, we will always assume $Y_p = 0.23$. We define $T = (1+z)2.7$ K so that T represents the effective photon temperature for the nonequilibrium photon distribution. Thus, the ratio T_e/T plays an important role only in cases where the electron temperature is not tightly coupled to the photon temperature.

Elastic Compton scattering cannot change the number of photons, but only redistribute them in frequency. This may be directly verified by integrating the Kompaneets equation (1) to form the change in the total number density n_γ :

$$\left(\frac{dn_\gamma}{dt} \right)_K \propto \int dx_e x_e^2 \left(\frac{\partial n}{\partial t} \right)_K = 0. \quad (4)$$

The kinetic equilibrium solution is therefore a Bose-Einstein spectrum at the electron temperature:

$$n_{\text{BE}} = \frac{1}{e^{x_e + \mu} - 1}, \quad (5)$$

where μ is the dimensionless chemical potential. That Eq. (5) is the equilibrium solution of the Kompaneets equation can easily be verified by its insertion into the Kompaneets equation (1). A true static solution to the Kompaneets equation includes only $\mu > 0$ due to the unphysical behavior of the negative chemical potential spectrum at frequencies $x_e \leq |\mu|$. However, with the inclusion of bremsstrahlung and double Compton scattering, we shall see that it is possible to obtain quasistatic spectra with $\mu < 0$ for the high-frequency regime $x_e \gg |\mu|$.

The electron temperature is given by [11,12]

$$T_e = \frac{1}{4} \frac{h}{k} \frac{\int v^4 n(n+1) dv}{\int v^3 n dv}, \quad (6)$$

where we have assumed that the electron temperature is governed by the photons through elastic Compton scattering. This equilibrium temperature is attained on a time scale that is much shorter than any process considered here: namely,

$$t_{e\gamma} = \frac{3m_e c}{4\sigma_T \epsilon} \approx 7.63 \times 10^{19} (1+z)^{-4} \Theta_{2.7}^{-4} \text{ s}. \quad (7)$$

Here ϵ is the energy density of the photons. Note that in the presence of a Bose-Einstein spectrum, the electron temperature does not change as is required of an equilibrium solution. The short time scale involved in Eq. (7) simply reflects the fact that $n_\gamma \gg n_e$. Thus, the time scale for a given electron to Compton scatter off a photon is much shorter than that of a given photon to scatter with an electron. Alternatively, the heat capacity of the photons is much greater than that of the electrons. Thus the total energy density of the photons, ignoring expansion, effectively does not change:

$$\left(\frac{d\epsilon}{dt} \right)_K \propto \int dx_e x_e^3 \left(\frac{\partial n}{\partial t} \right)_K = 0, \quad (8)$$

as we can see by integrating Eq. (1) twice by parts and employing Eq. (6). Under elastic Compton scattering and cosmological conditions, then, the number and energy density of the photons changes only due to the expansion.

True thermodynamic equilibrium, of course, requires that the photons form a Planck distribution. However, an arbitrary spectrum cannot relax to a blackbody distribution via elastic Compton scattering. It will not, in general, contain the same number of photons as a blackbody of the equivalent temperature. In order to obtain a blackbody distribution, number-changing processes, i.e., to lowest-order bremsstrahlung, $e^- + X \rightarrow e^- + X + \gamma$ (where X is an ion), and/or inelastic, henceforth referred to as double Compton scattering $e^- + \gamma \rightarrow e^- + \gamma + \gamma$, must be effective. We neglect higher-order Compton scattering.

Much of the early work on this subject [13–17] as-

sumed that bremsstrahlung is the dominant photon-creating process in the early Universe. The kinetic equation for bremsstrahlung is well known [3]:

$$\left[\frac{\partial n}{\partial t} \right]_{\text{br}} = (n_e \sigma_{TC}) Q \frac{g(x_e)}{e^{x_e}} \frac{1}{x_e^3} [1 - n(e^{x_e} - 1)], \quad (9)$$

where

$$Q = \frac{4\pi}{(2\pi)^{7/2}} \left[\frac{kT_e}{m_e c^2} \right]^{-1/2} \alpha \sum n_i Z_i^2 \left[\frac{hc}{kT_e} \right]^3.$$

Here n_i is number density of ions with atomic number Z_i , and α is the fine-structure constant. For a H+He plasma, $\sum n_i Z_i^2 = n_B$. The Gaunt factor $g(x_e)$ is given by

$$g(x_e) \simeq \begin{cases} \ln(2.25/x_e), & x_e \leq 0.37, \\ \pi/\sqrt{3}, & x_e \geq 0.37. \end{cases} \quad (10)$$

We will find it convenient to express these equations as

$$\left[\frac{\partial n}{\partial t} \right]_{\text{br}} = \frac{1}{t_{\text{br}}} \frac{g(x_e)}{e^{x_e}} \frac{1}{x_e^3} [1 - n(e^{x_e} - 1)], \quad (11)$$

where

$$t_{\text{br}} = 3.81 \times 10^{23} (1 - Y_p/2)^{-1} (\Omega_B h^2)^{-2} \times \Theta_{2.7}^{7/2} \left[\frac{T_e}{T} \right]^{7/2} z^{-5/2} \text{ s}. \quad (12)$$

As we can see from the scaling of Eq. (12), in a low baryon density universe as implied by nucleosynthesis constraints [18], $0.011 \leq \Omega_B h^2 \leq 0.016$, bremsstrahlung is rather inefficient. Double Compton scattering cannot be neglected under such conditions. Lightman [3] first derived the kinetic equation for double Compton scattering:

$$\begin{aligned} \left[\frac{\partial n}{\partial t} \right]_{\text{DC}} &= n_e \sigma_{TC} \frac{4\alpha}{3\pi} \left[\frac{kT_e}{m_e c^2} \right]^2 \frac{1}{x_e^3} [1 - n(e^{x_e} - 1)] \\ &\quad \times \int dx_e x_e^4 (1+n)n \\ &= \frac{1}{t_{\text{DC}}} I(t) \frac{1}{x_e^3} [1 - n(e^{x_e} - 1)], \end{aligned} \quad (13)$$

where

$$t_{\text{DC}} = 6.96 \times 10^{39} (1 - Y_p/2)^{-1} (\Omega_B h^2)^{-1} \times \Theta_{2.7}^{-2} \left[\frac{T_e}{T} \right]^{-2} z^{-5} \text{ s}, \quad (14)$$

and

$$I(t) = \int dx_e x_e^4 (1+n)n. \quad (15)$$

The kinetic equation (13) is only strictly valid for $x_e < 1$ since its derivation assumes that the photon produced is lower in energy than the incoming photon. Double Compton scattering is, of course, inefficient at creating photons above the mean energy of the photons in the spectrum. However, we will only be concerned with the effects of double Compton scattering in the low-frequency regime where it is efficient. Comparing Eqs. (12) and (14)

for the time scales, we see that in a low $\Omega_B h^2$ universe and at sufficiently high redshifts, double Compton scattering will dominate over bremsstrahlung.

The full kinetic equation to lowest order now reads

$$\left[\frac{\partial n}{\partial t} \right] = \left[\frac{\partial n}{\partial t} \right]_K + \left[\frac{\partial n}{\partial t} \right]_{\text{DC}} + \left[\frac{\partial n}{\partial t} \right]_{\text{br}}. \quad (16)$$

Notice that the equilibrium solution for the full kinetic equation includes only the Planck distribution, i.e., a Bose-Einstein spectrum with $\mu=0$.

We wish to examine the case in which an initial blackbody distribution of photons is perturbed by the injection of energy at some epoch z_h , specifically an arbitrary injection of photons. For simplicity, we take the injection to be instantaneous. We then follow the evolution of the perturbed spectrum until recombination z_{rec} , at which time the number density of free electrons drops precipitously and distortions are essentially frozen into the spectrum.

Evolution of an arbitrary spectrum under the full kinetic equation must, in general, be solved numerically. We employ a fully implicit iterative modified Youngs approach to solve Eq. (16) numerically [19]. Analytic approximations do exist in various limiting cases (Secs. IV, V, and VI) where quasiequilibrium holds. We shall compare them to the numerical solutions and examine their range of applicability. We shall also examine the case of a negative chemical potential Bose-Einstein spectrum which must be handled entirely numerically.

III. THERMALIZATION TIME SCALES

In order to discuss the thermalization and evolution of spectral distortions, we must examine the relative and absolute rates of these processes. A qualitative examination of the full kinetic equation (16) shows that, at high redshifts, elastic and double Compton scattering will dominate over bremsstrahlung. Furthermore, double Compton scattering, as well as bremsstrahlung, becomes increasingly efficient as frequency decreases. The rate of elastic Compton scattering is, on the other hand, independent of frequency. We therefore expect that at high enough redshifts, double Compton scattering will be responsible for creating and/or absorbing photons at low frequencies, while elastic Compton scattering will redistribute them in frequency. The net effect will be that a blackbody distribution is efficiently established. At lower redshifts, we expect that double Compton scattering and bremsstrahlung will be efficient only at very low frequencies. Thus there will be an insufficient number of photons to create a blackbody distribution except at the lowest frequencies. Elastic Compton scattering will instead establish a Bose-Einstein spectrum at high frequencies. At redshifts near combination, we expect that even elastic Compton scattering will be ineffective at thermalizing distortions. Spectral distortions at high frequencies will be frozen in. At low frequencies, bremsstrahlung will dominate and be able to return the spectrum to blackbody.

Now let us examine the rates quantitatively. We may extend the analysis of Danese and De Zotti for brems-

strahlung [2] to include double Compton scattering. Consider a spectrum which at a given frequency x_e has no photons. We wish to find the characteristic time scale for which bremsstrahlung and/or double Compton scattering can create a Planck distribution. It is convenient to define the quantities

$$\begin{aligned} y_{\text{br}}^* &= \int_{t_h}^t dt' t_{\text{br}}^{-1} g(x_e) / (x_e^3 e^{x_e}), \\ y_{\text{DC}}^* &= \int_{t_h}^t dt' t_{\text{DC}}^{-1} I(t') / x_e^3. \end{aligned} \quad (17)$$

In general, $I(t)$ involves the integral over the spectrum given by Eq. (15). However, the integral is dominated by the high-frequency region $x_e > 1$. Since we are considering $x_e < 1$ and assuming that an equilibrium distribution has already been formed at high frequencies, we may assume $I(t) \simeq \text{const}$. For estimation purposes, we will use $I(t) \simeq I_P = 25.976$, the value for a Planck distribution. Note that there is a fundamental difference between bremsstrahlung and double Compton scattering. For double Compton scattering to create photons, there must already be photons present in the spectrum. Double Compton scattering itself cannot create a Planck distribution *ex nihilo*.

Considering the processes independently, we can now write the kinetic equation for double Compton scattering or bremsstrahlung as

$$\frac{\partial n}{\partial y_{\text{br/DC}}^*} = 1 - n(e^{x_e} - 1). \quad (18)$$

Assuming no photons initially, $n(y^* = 0) = 0$, we find that the solution of this equation is

$$n = (e^{x_e} - 1)^{-1} [1 - \exp(-y_{\text{br/DC}})], \quad (19)$$

where

$$y_{\text{br/DC}} \equiv y_{\text{br/DC}}^* (e^{x_e} - 1) \quad (20)$$

is the optical depth of the Universe to absorption by bremsstrahlung or double Compton scattering. A Planck distribution at frequency x_e is thus established on a characteristic time scale:

$$\begin{aligned} \tau_{\text{br}} &\simeq \tau_{\text{exp}} / y_{\text{br}} \simeq t_{\text{br}} \frac{e^{x_e}}{g(x_e)} \frac{x_e^3}{e^{x_e} - 1}, \\ \tau_{\text{DC}} &\simeq \tau_{\text{exp}} / y_{\text{DC}} \simeq t_{\text{DC}} \frac{1}{I_P} \frac{x_e^3}{e^{x_e} - 1}, \end{aligned} \quad (21)$$

where τ_{exp} is the expansion time. Note that the expression for the double Compton scattering thermalization time scale is valid for $x_e < 1$ only.

Above the redshift at which these rates become equal, double Compton should dominate over bremsstrahlung as the crucial photon-creating process. This occurs at

$$z_{\text{DC,br}} \simeq 8.69 \times 10^5 (\Omega_B h^2)^{2/5} \Theta_{2.7}^{-11/5} g(x_e)^{2/5}, \quad x_e \ll 1, \quad (22)$$

which is roughly independent of frequency due to the fact that the frequency dependences of the two rates are simi-

lar. For estimation purposes, we have assumed that $T_e \simeq T$.

On the other hand, the time scale for establishing a Bose-Einstein distribution via elastic Compton scattering [2],

$$\tau_K = t_K / 4, \quad (23)$$

is itself independent of frequency. We therefore expect that the number-changing processes will dominate over elastic Compton scattering below the frequency at which the rates are equal. For $x_e \ll 1$, we may approximate this as

$$\begin{aligned} x_{c,\text{br}} &\simeq 8.0 \times 10^1 g(x_{c,\text{br}})^{1/2} (\Omega_B h^2)^{1/2} \Theta_{2.7}^{-9/4} z^{-3/4}, \\ x_{c,\text{DC}} &\simeq 3.0 \times 10^{-6} \Theta_{2.7}^{1/2} z^{1/2}. \end{aligned} \quad (24)$$

where $\tau_{\text{br}}(x_{c,\text{br}}) = \tau_K(x_{c,\text{br}})$ and $\tau_{\text{DC}}(x_{c,\text{DC}}) = \tau_K(x_{c,\text{DC}})$. Note that $g(x_e)$ is only logarithmically dependent on frequency. Let us define

$$x_c^2 = x_{c,\text{br}}^2 + x_{c,\text{DC}}^2. \quad (25)$$

Above the frequency x_c , the spectrum will be Bose-Einstein given sufficient time to establish equilibrium. Below this frequency, the spectrum returns to a Planck distribution. Thus, Eq. (25) defines the critical frequency at which the spectrum assumes a form intermediate between the two equilibrium configurations. The shape of the spectrum in this intermediate zone will be the topic of Sec. V.

However, when the thermalization times become longer than the expansion time these processes become inefficient. The expansion time is given by

$$\begin{aligned} \tau_{\text{exp}} &\equiv \frac{a}{da/dt} \\ &\simeq 4.88 \times 10^{19} (z + z_{\text{eq}})^{-1/2} \Theta_{2.7}^{-2} z^{-3/2} \text{ s}, \end{aligned} \quad (26)$$

where $z_{\text{eq}} = 2.50 \times 10^4 \Omega h^2 \Theta_{2.7}^{-4}$ is the redshift of matter-radiation equality. When the thermalization time for elastic Compton scattering is greater than the expansion time, not even a Bose-Einstein distribution can be established. This occurs for values of z less than

$$z_K \simeq 7.09 \times 10^3 (1 - Y_p / 2)^{-1/2} (\Omega_B h^2)^{-1/2} \Theta_{2.7}^{1/2}, \quad (27)$$

for $z \gg z_{\text{eq}}$. Furthermore, we can also define the frequencies at which the thermalization time scales of the photon-creating processes are equal to the expansion time:

$$\begin{aligned} x_{\text{exp,br}} &\simeq 1.1 \times 10^{-2} (1 - Y_p / 2)^{-1/2} g(x_{\text{exp,br}})^{1/2} \\ &\quad \times \Omega_B h^2 \Theta_{2.7}^{-11/4} z^{1/4}, \\ x_{\text{exp,DC}} &\simeq 4.3 \times 10^{-10} (1 - Y_p / 2)^{-1/2} (\Omega_B h^2)^{1/2} \\ &\quad \times \Theta_{2.7}^{-1} z^{3/2}, \end{aligned} \quad (28)$$

where $\tau_{\text{br}}(x_{\text{exp,br}}) = \tau_{\text{exp}}$ and $\tau_{\text{DC}}(x_{\text{exp,DC}}) = \tau_{\text{exp}}$. Again, define

$$x_{\text{exp}}^2 = x_{\text{exp,br}}^2 + x_{\text{exp,DC}}^2. \quad (29)$$

Thus, even at $x_e < x_c$, if $x_e > x_{\text{exp}}$, a Planck distribution

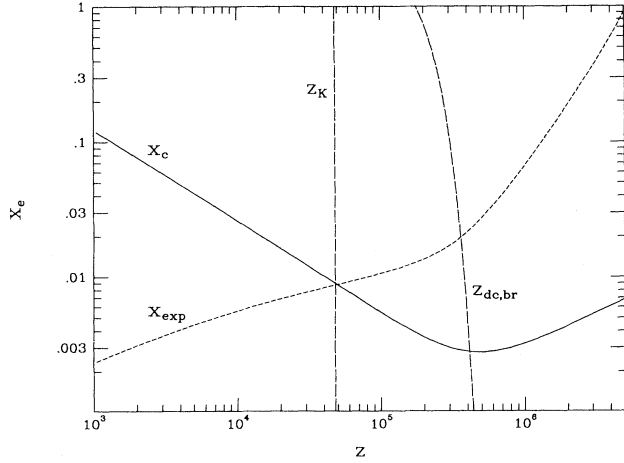


FIG. 1. Critical frequencies as a function of redshift for $\Omega h^2=0.25$, $\Omega_B h^2=0.025$. Solid line is x_c , dashed line is x_{exp} , long dashed lines represent critical redshifts as labeled.

may still not be established due to the ineffectiveness of the number-changing processes with respect to the expansion. Note, however, that if $z > z_K$ a Planck distribution is *not* established for all $x_e < x_{\text{exp}}$ despite the relative effectiveness of the number-changing processes. This is because x_{exp} is the frequency at which a Planck distribution would be formed in the absence of elastic Compton scattering. If elastic Compton scattering is effective, it will compete with the number-changing processes by scattering upward in frequency photons which would otherwise contribute to the establishment of a Planck distribution at $x_e < x_{\text{exp}}$. Thus for $z > z_K$, the frequency at which a Planck distribution is established is x_c rather than x_{exp} .

Figure 1 graphically displays these critical frequencies and redshifts for the representative choice of $\Omega_B h^2=0.025$. Notice the transition to double Compton scattering dominance for $z > z_{\text{DC,br}}$ and small deviations from the simple power-law approximations given by Eqs. (24) and (28) for $x_e \simeq 1$ and $z < z_{\text{eq}}$. Here $\Omega h^2=0.25$, but this parameter plays only a small role in the thermalization process, entering only for $z < z_{\text{eq}}(\Omega h^2)$.

IV. HIGH-FREQUENCY SPECTRUM

As we have seen, at high frequencies, the spectrum should resemble a Bose-Einstein distribution. In fact, if the photon-creating processes are much slower than elastic Compton scattering, the chemical potential is directly related to the parameters of the injection. As shown in Eqs. (4) and (8), under elastic Compton scattering neither the energy nor the number of photons changes. Therefore, we can relate the resultant chemical potential to the number and energy density of the photons injected. In prior treatments [2,16,17,20], it has been customarily assumed that energy injection occurs *with a negligible change in the number of photons*. This assumption is true for a broad range of injection mechanisms including direct heating of the electrons and Klein-Nishina cascades [21]. However, it does not describe the most gen-

eral type of injection. We can easily extend the treatment to the case where the injection itself involves a significant number of photons (e.g., radiative particle decay and free-free emission of a hot plasma).

The energy in a Bose-Einstein distribution can be expressed as

$$\epsilon_{\text{BE}} = \frac{8\pi h}{c^3} \int n_{\text{BE}} v^3 dv = \epsilon_P(T_e) f(\mu), \quad (30)$$

where

$$f(\mu) \simeq \begin{cases} \frac{6}{I_3} \exp(-\mu), & \mu \gg 1, \\ 1 - 3 \frac{I_2}{I_3} \mu, & \mu \ll 1, \end{cases} \quad (31)$$

and $\epsilon_P(T_e) = aT_e^4 = 4\sigma_B T_e^4/c$, the energy density of blackbody radiation, with σ_B being the Stefan-Boltzmann constant. Similarly, the number density is given by

$$n_{\gamma\text{BE}} = \frac{8\pi}{c^3} \int n_{\text{BE}} v^2 dv = n_{\gamma P}(T_e) \phi(\mu), \quad (32)$$

where

$$\phi(\mu) \simeq \begin{cases} \frac{2}{I_2} \exp(-\mu), & \mu \gg 1, \\ 1 - 2 \frac{I_1}{I_2} \mu, & \mu \ll 1, \end{cases} \quad (33)$$

with $n_{\gamma P}(T) = (I_2/I_3) aT^3/k$. Here the constants I_n are defined by the Reimann ζ function as follows:

$$I_n = \int_0^\infty dx \frac{x^n}{e^x - 1} = n! \zeta(n+1),$$

e.g., $I_1 \simeq 1.645$, $I_2 \simeq 2.404$, $I_3 \simeq 6.494$.

The number of photons in a Bose-Einstein distribution decreases with increasing chemical potential. In particular, a spectrum with $\mu < 0$ has more photons than a blackbody, $\mu = 0$; conversely, a spectrum with $\mu > 0$ has fewer photons. Parenthetically, note that we can express the double Compton scattering integral [Eq. (15)] as

$$I_{\text{BE}} = \int dx_e x_e^4 (1 + n_{\text{BE}}) n_{\text{BE}} = 4I_3 f(\mu), \quad (34)$$

for the case of a Bose-Einstein distribution.

Now if we require energy and number conservation, Eqs. (30) and (32) tell us

$$\epsilon_{\text{BE}} = aT_e^4 f(\mu) = \epsilon_P(T_i) (1 + \delta\epsilon/\epsilon) = aT_i^4 (1 + \delta\epsilon/\epsilon), \quad (35)$$

and

$$\begin{aligned} n_{\gamma\text{BE}} &= \frac{aT_e^3}{k} \frac{I_2}{I_3} \phi(\mu) \\ &= n_{\gamma P} \left[1 + \frac{\delta n}{n} \right] = \frac{aT_i^3}{k} \frac{I_2}{I_3} \left[1 + \frac{\delta n}{n} \right], \end{aligned} \quad (36)$$

where T_i represents the temperature of the radiation before injection. For small chemical potentials, we may solve Eqs. (35) and (36) simultaneously to obtain

$$\mu_{\text{pred}}(z_h) \simeq \frac{1}{2.143} \left[3 \frac{\delta\epsilon}{\epsilon} - 4 \frac{\delta n}{n} \right], \quad \mu \ll 1, \quad (37)$$

to first order in the perturbations. This is the chemical potential established near the epoch of heating z_h after a time $t > \tau_K$ but before photon-creating processes have taken effect. We will discuss the action of such processes in altering the chemical potential in Sec. VI. Equation (37) has been checked numerically in epochs where photon-creating processes are entirely negligible. For such regimes, the agreement is excellent for $10^{-1} > \mu > 0$ and satisfactory for $0 > \mu > -10^{-2}$ and $1 > \mu > 10^{-1}$.

Let us examine qualitatively the behavior of Eq. (37). Injection of energy tends to heat the electrons and cause $T_e > T_i$. Since the number of photons in a blackbody is proportional to T^3 , this would make the spectrum underpopulated with respect to the blackbody. However, this deficit of photons can be partially or wholly compensated by the number of photons involved in the injection. In fact, unlike the case considered previously where $\delta n/n \ll 1$, the chemical potential can become negative if the energy is injected at a frequency $x_h \lesssim 3.6$. An even more curious effect happens if energy is injected either at, or symmetrically about, this critical value. In this case, the number of photons and the corresponding energy injected is just enough so that the electrons are heated to a temperature at which there are exactly enough photons to create a blackbody spectrum. This implies that an arbitrarily large amount of energy may be injected at this critical frequency and, given sufficient time for the photons to redistribute, still leave $\mu=0$; i.e., the spectrum will remain a perfect blackbody. This effect will be considered more carefully in Sec. V. Presumably, however, any physically realistic process will inject photons over a wide range of frequencies and destroy this balance [22].

In the case of negative chemical potentials, we clearly cannot ignore number-changing processes at any redshift or baryon density since the spectrum becomes unphysical if $x_e < |\mu|$. Although it may be that double Compton scattering and bremsstrahlung are ineffective near the frequency of injection, they play a crucial role in the evolution of the spectrum. Elastic Compton scattering will move excess photons downward in frequency until they can be absorbed by double Compton scattering and/or bremsstrahlung. The case of low-frequency injection was briefly considered by Illarionov and Sunyaev [16] where the down scattering was said to lead to ‘‘Bose-Einstein condensation’’; they, however, did not consider the form of the spectrum that results from the inclusion of photon-absorbing processes. Here we show that the spectrum is also Bose-Einstein at high frequencies $x_e \gg x_c$ but with *negative* chemical potential. However, although Eq. (37) tells us that these negative chemical potentials should be possible, it cannot predict the value of the chemical potential since it explicitly ignores crucial processes. We expect, however, that a quasiequilibrium solution can only exist if $|\mu|$ is less than or equal to the frequency at which the photon absorbing processes are

effective, i.e., $|\mu| < x_{\text{expt}}(z_\mu)$, where z_μ is some characteristic redshift at which such processes can affect the overall spectrum. We will discuss these issues further in Sec. VI. If this condition is not satisfied, elastic Compton scattering will continue to scatter photons downward in frequency. Thus the spectrum will evolve further as long as elastic Compton scattering is effective or until this condition is met. We expect then that the range of negative chemical potentials obtainable is far more limited than that of positive chemical potentials. Given this suppression of large negative chemical potentials, one might worry that the presence of a small to vanishing negative chemical potential in the cosmic background radiation today does not serve to limit low-frequency injection scenarios. For example, naive constraints on particles that decay while relativistic [23] may be invalid. Although relativistic decay cannot be simply modeled as instantaneous energy injection, it results in a negative chemical potential Bose-Einstein distribution. Thus our study of the evolution of such spectra is relevant for this as well as other processes. In Sec. VI, we will see, however, that in the limit of small present day distortions the naive estimates can, in general, be employed.

Therefore, an examination of negative chemical potentials requires a numerical analysis due to this instability near $x_e \simeq |\mu|$. Numerical analysis is also required to consider the transition to a Planck distribution at low frequencies. This is particularly important for comparison with observation since a Bose-Einstein spectrum deviates most strongly from a Planck distribution at low frequencies $x_e \leq |\mu|$. It is thus important to determine at what frequency the spectrum returns to a Planck distribution and what deviations we might expect in this region. This will be the subject of Sec. V. Furthermore, in order to examine the time dependence of the high-frequency spectrum, i.e., the chemical potential, in the general case, a numerical treatment is required (Sec. VI).

Note finally that Eq. (37) tells us that the establishment of the Bose-Einstein spectrum is independent of the precise form of the injection. It depends only on the *total* number and energy density of the photons injected. This is a very powerful result. For instance, direct heating of the electrons is equivalent to injecting a negligible number of high-energy photons. Furthermore, an arbitrary distribution of injected photons can be parametrized by the single quantity $\mu(\delta n_\gamma/n_\gamma, \delta\epsilon/\epsilon)$ alone. This has been tested numerically and is valid for $\mu_{\text{pred}}(z_h) > 0$. We will discuss the ‘‘breakdown’’ of Eq. (37) for predictions of zero and negative chemical potentials below (Secs. V and VI, respectively). Given the independence of the evolution to the specifics of the injection for most cases, it is convenient to employ injections which may be represented as ‘‘ δ functions’’ (i.e., peaked functions localized in frequency) located at some frequency x_h . For the above argument to hold, we must have $x_h > x_c$ so that bremsstrahlung and double Compton scattering can be ignored during the initial thermalization.

V. LOW-FREQUENCY SPECTRUM

Analytic work has been performed on the form of the low-frequency spectrum [4,14,16]. However, the approxi-

mations employed are only strictly valid for $z \gg z_K$. Notice that this also implies $x_c \ll x_{\text{expt}}$ and thus both elastic Compton scattering and photon-creating processes may be considered effective at the critical frequency. In order to examine the low-frequency behavior of the present day spectrum, we must evolve the spectrum numerically until last scattering $z = z_{\text{rec}} < z_K$ [24]. The approximations to the low-frequency spectrum were originally derived [14] to examine the time evolution of the chemical potential (see Sec. VI below). In this case, it is valid to consider the behavior up to $z = z_K$ since it is elastic Compton scattering that is responsible for moving the photons produced at low frequencies up in frequency or moving excesses at high frequencies down. It therefore plays a crucial role in the reduction of the chemical potential. If $z < z_K$, the chemical potential, i.e., the high-frequency distortion, is effectively frozen in. However, even for a study of possible present day low-frequency behavior, it is still useful to examine these analytic approximations in order to guide the interpretation of the numerical solutions.

The basic technique, first employed by Zel'dovich and Sunyaev [14] and extended by Danese and De Zotti [4] to include double Compton scattering, involves the assumption that one or more of the three processes are effective enough to establish quasistatic conditions:

$$\left[\frac{\partial n}{\partial t} \right] = \left[\frac{\partial n}{\partial t} \right]_K + \left[\frac{\partial n}{\partial t} \right]_{\text{br}} + \left[\frac{\partial n}{\partial t} \right]_{\text{DC}} \simeq 0; \quad (38)$$

i.e., the rate of change of the spectrum can be considered slow. Equation (38) is valid for the entire spectrum only when $z \gg z_K$.

Note that we may always reexpress the spectrum in terms of a frequency-dependent ‘‘chemical potential,’’

$$n(x_e) = \frac{1}{\exp[x_e + \mu'(x_e)] - 1}, \quad (39)$$

without loss of generality. The complete kinetic equation in the quasistatic approximation, i.e., Eq. (38), then becomes

$$\begin{aligned} & \frac{1}{x_e^2} \frac{d}{dx_e} \left[x_e^4 \frac{\exp[x_e + \mu'(x_e)]}{\{\exp[x_e + \mu'(x_e)] - 1\}^2} \frac{d\mu'}{dx_e} \right] \\ &= \left[\frac{t_K}{t_{\text{br}}} \frac{g(x_e)}{e^{x_e}} + \frac{t_K}{t_{\text{DC}}} I_{\text{BE}} \right] \\ & \times \frac{e^{x_e}}{x_e^3} \frac{\exp[\mu'(x_e)] - 1}{\exp[x_e + \mu'(x_e)] - 1}. \end{aligned} \quad (40)$$

If we make the further approximation that $g(x_e) \simeq g(x_{c,\text{br}})$, we may express this as

$$\begin{aligned} & \frac{1}{x_e^2} \frac{d}{dx_e} \left[x_e^4 \frac{\exp[x_e + \mu'(x_e)]}{\{\exp[x_e + \mu'(x_e)] - 1\}^2} \frac{d\mu'}{dx_e} \right] \\ &= 4x_c^2 \frac{e^{x_e}}{x_e^3} \frac{\exp[\mu'(x_e)] - 1}{\exp[x_e + \mu'(x_e)] - 1}, \end{aligned} \quad (41)$$

for $x_e \ll 1$.

For $\mu'(x_e) \ll x_e$, Eq. (41) is easily solved:

$$\mu'(x_e) = C_1 \exp(-2x_\mu/x_e), \quad (42)$$

where

$$x_\mu = x_c(z) \quad (43)$$

for redshifts at which quasiequilibrium can be maintained. We have taken the solution corresponding to $\mu'(0) = 0$, since at very low frequency the spectrum is a Planck distribution.

At high frequencies, $x_e \gg x_c$, we expect that the spectrum will be Bose-Einstein with chemical potential μ . Thus if $\mu < x_c$, the two solutions must match at the junction i.e., $C_1 = \mu$. If $\mu > x_c$, C_1 must be found numerically. Illarionov and Sunyaev [16] give $C_1 \simeq 3x_{c,\text{br}}$, for $\mu > x_c$ and $x_{c,\text{br}} \gg x_{c,\text{DC}}$. We have checked this for limiting cases in which bremsstrahlung dominates over double Compton scattering and $z \gg z_K$ and found rough agreement $C_1 \simeq \text{few} \times x_{c,\text{br}}$. Given the observational constraint on the chemical potential, we need not consider the case of large chemical potentials for $z < z_K$.

It is convenient to describe these distortions from a blackbody spectrum as a ratio of the frequency-dependent effective temperature to the temperature of the Wien tail T_0 . Assuming that the Wien tail is Bose-Einstein in form, we require $T_0 = T_e$ up until recombination, and thus

$$\frac{T}{T_0} = \frac{x_e}{\ln[(1+n)/n]}. \quad (44)$$

Notice that a spectrum of the form given by Eq. (42) obtains its peak distortions in $\log_{10}(T/T_0)$ at

$$x_{\text{peak}} = 2x_\mu, \quad \mu < x_c(z) \quad (45)$$

at a value

$$\left[\log_{10} \frac{T}{T_0} \right]_{\text{max}} = \log_{10} \left[1 + \frac{C_1}{x_{\text{peak}} e} \right] = \log_{10} \left[1 + \frac{\mu}{2x_\mu e} \right]. \quad (46)$$

The quasi-static approximation must, however, break down at redshifts $z_{\text{rec}} < z \lesssim z_K$ due to the freeze-out of elastic Compton scattering. Freeze-out, however, is not instantaneous at z_K and photon-creating processes remain effective at low frequencies. Thus the spectrum should continue to evolve beyond this so called ‘‘freeze-out’’ and display distortions from the form given by Eq. (42). Figure 2 shows the evolution of a spectrum, with $\mu(z_h) > 0$ ($\delta n_\gamma/n_\gamma = 2.5 \times 10^{-3}$, $\delta\epsilon/\epsilon = 5.5 \times 10^{-3}$) from the heating epoch $z_h = 6 \times 10^5$ to recombination. In Fig. 2(a), the initial δ -function injection is thermalized by elastic Compton scattering and forms a Bose-Einstein distribution at high frequencies on a time scale comparable to τ_K . Figure 2(b) displays the further quasistatic evolution of the spectrum and the gradual freeze-out of the processes for $z \lesssim z_K \simeq 5 \times 10^4$. Notice that significant evolution of the low-frequency spectrum occurs at $z_{\text{rec}} < z < z_K$ where quasistatic equilibrium cannot be maintained.

It is instructive to consider the evolution of this spectrum in some detail. Figure 2(a) displays the establishment of a Bose-Einstein spectrum via elastic Compton scattering. At the epoch of heating, energy is injected

which rapidly heats the electrons. Initially, the temperature of the photons is lower than T_e across the spectrum. Therefore, there is a deficit of photons in comparison with a Planck distribution at temperature T_e . Elastic Compton scattering off hot electrons then causes low-frequency photons to scatter upward in frequency. The high-frequency deficit is consequently reduced at the expense of the low frequency until a Bose-Einstein distribution is attained at high frequencies. At this point, rapid evolution of the spectrum halts and quasiequilibrium is attained. Bremsstrahlung, and at the low redshifts considered here, to a lesser extent double Compton scattering, supplies photons at low frequencies. Thus the low-frequency spectrum deviates from a perfect Bose-Einstein spectrum by returning to a blackbody distribution at $x_e \ll x_c(z)$. The overall spectrum is described well by (42). For example, at $z=4.75 \times 10^5$, $x_{\text{peak}} \approx 6 \times 10^{-3}$

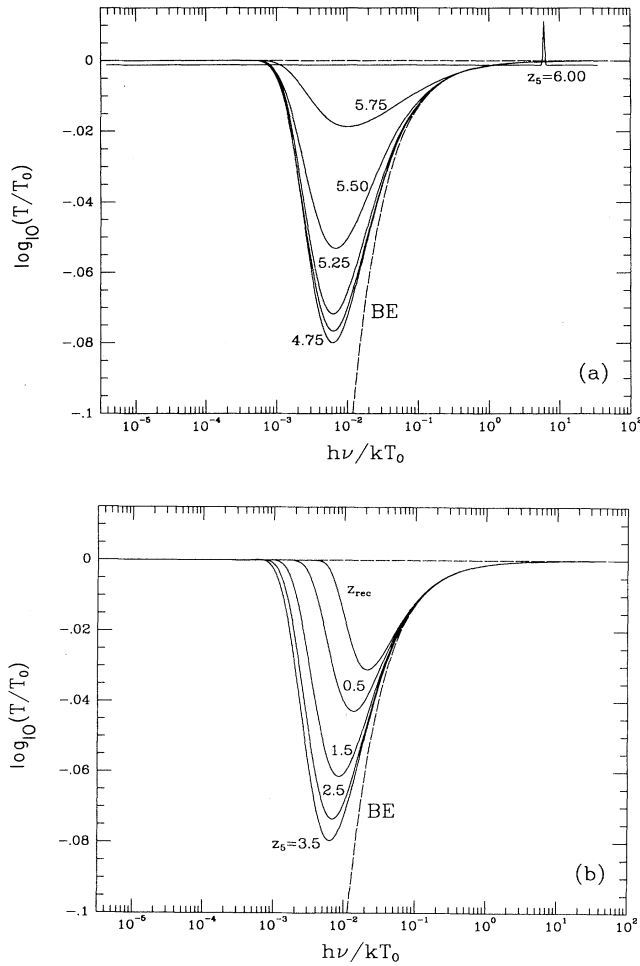


FIG. 2. Time evolution of low-frequency spectrum, $\mu > 0$. Initial spectrum: injection at $x_h=6$, $z_h=6 \times 10^5$ with $\delta n_\gamma/n_\gamma=2.5 \times 10^{-3}$, $\delta\epsilon/\epsilon=5.5 \times 10^{-3}$, for $\Omega h^2=0.25$, $\Omega_B h^2=0.025$. (a) Establishment of the Bose-Einstein spectrum, $4.75 \times 10^5 < z < 6.00 \times 10^5$, where $z_{[s]}=z/10^5$. Unlabeled curve represents $z=5.0 \times 10^5$. (b) Quasistatic evolution and freeze-out, $z_{\text{rec}} < z < 3.5 \times 10^5$. Long dashes represents best fit Bose-Einstein spectrum and the undistorted Planck distribution.

whereas $2x_c=5.6 \times 10^{-3}$. The peak value is slightly underestimated by (46) due to the finite rate of elastic Compton scattering. The peak amplitude of distortions is $\log_{10}(T/T_0)=7.99 \times 10^{-3}$ whereas Eq. (46) predicts 7.96×10^{-3} . This deviation will grow into a significant effect by z_{rec} . Note also that the chemical potential is accurately predicted by Eq. (37). The high-frequency spectrum at $z=4.75 \times 10^5$ has a chemical potential $\mu=3.05 \times 10^{-3}$ whereas $\mu_{\text{pred}}=3.06 \times 10^{-3}$.

Figure 2(b) displays the subsequent quasistatic evolution of the spectrum. At $x_c(z) < x_e < x_{\text{expt}}(z)$, photons are effectively produced and can be scattered up to affect the high-frequency spectrum (i.e., reduce the chemical potential). Low-frequency photons produced at $x_e < x_c(z)$ are absorbed by inverse bremsstrahlung and inverse double Compton scattering before they can be scattered up in frequency. Under the joint action of elastic Compton scattering and the photon-creating processes, the spectrum evolves under Eq. (42). The peak of the distortion moves to higher frequencies since photons created by bremsstrahlung and double Compton scattering reduce the low-frequency distortions. High-frequency distortions are also affected as the created photons are scattered to higher and higher frequencies. However, at these low redshifts there is insufficient time to alter the chemical potential significantly (see Sec. VI).

Near z_K , elastic Compton scattering becomes ineffective at moving photons upwards in frequency. Thus, the distortions during this epoch are larger than Eq. (42) would imply. The peak of the distortion also lags behind $2x_c(z)$ and by recombination only attains a frequency marginally larger than $2x_c(z_K)$. For the spectrum in Fig. 2, $x_{\text{peak}}(z_{\text{rec}})=2.1 \times 10^{-2}$ and $2x_c(z_K)=1.8 \times 10^{-2}$. Thus, a reasonable approximation to the low-frequency spectrum would be to employ the form of (42) with x_μ replaced by $x_c(z_K)$. This is equivalent to assuming that quasistatic equilibrium is strictly maintained until z_K whereupon freeze-out occurs instantaneously and uniformly across the spectrum.

Now let us examine the deviations from this approximation. Qualitatively we expect significant deviations since at $z \lesssim z_K$ the low-frequency spectrum can still evolve under photon-creating processes whereas the high-frequency spectrum is essentially frozen in. Figure 3 shows the spectral distortions obtained from evolving a spectrum with $\mu < x_c(z)$, ($\delta n_\gamma/n_\gamma=1.2 \times 10^{-3}$, $\delta\epsilon/\epsilon=2.7 \times 10^{-3}$, $z_h=4 \times 10^5$) for $\Omega h^2=0.25$, $\Omega_B h^2=0.025$. The high-frequency spectrum fits the form of a Bose-Einstein spectrum with $\mu=1.521 \times 10^{-3}$ which agrees extremely well with predictions employing Eq. (37) ($\mu_{\text{pred}}=1.526 \times 10^{-3}$) due to the low redshift of heating. However, the low-frequency spectrum does show significant deviations from the predictions. Curve A shows the analytic prediction with $x_\mu=5.1 \times 10^{-3}$ which represents instantaneous freeze-out at $z \approx 2z_K$; curve B shows the predictions for $x_\mu=x_c(z_K)=9.0 \times 10^{-3}$, i.e., instantaneous freeze-out at $z=z_K$. Curve A fits the distortions above the peak and shows that these high-frequency distortions begin to freeze in at a redshift $z \approx 2z_K$. Below the peak, further evolution has

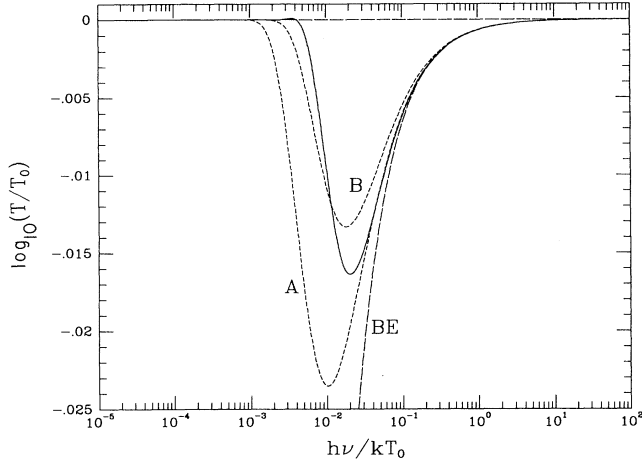


FIG. 3. Present day low-frequency spectrum for $\mu > 0$. Initial spectrum: injection with $\delta n_\gamma/n_\gamma = 1.2 \times 10^{-3}$, $\delta\epsilon/\epsilon = 2.7 \times 10^{-3}$ at $x_h = 6$, $z_h = 4 \times 10^5$ for $\Omega h^2 = 0.25$, $\Omega_B h^2 = 0.025$. Dashed lines represent the analytic predictions for instantaneous freeze-out at (A) $z \approx 2z_K$ and (B) $z = z_K$.

taken place but not sufficiently rapidly to follow *B*. Notice that above the peak, distortions are greater than those predicted by *B* due to the lack of evolution between $2z_K$ and z_{rec} of the high-frequency spectrum. The low-frequency distortions, on the other hand, are smaller than those predicted due to the further creation of low-frequency photons. Recall that at sufficiently low frequencies, photon-creating processes are effective all the way down to recombination. The location of the peak distortion $x_{\text{peak}} = 2.0 \times 10^{-2}$ is again only slightly greater than $2x_c(z_K) = 1.8 \times 10^{-2}$. In this case, the approximation $x_\mu = x_c(z_K)$ with Eq. (42) gives an adequate order of magnitude estimation of the distortions.

These effects are somewhat dependent on $\Omega_B h^2$, since, for a universe with high $\Omega_B h^2$, bremsstrahlung is more efficient. However, the time between z_K and z_{rec} in a high baryon density universe is smaller than that of a low baryon density one, and thus less evolution can take place. Furthermore, distortions at low frequency, though significant in terms of effective temperature, are small in terms of the physically meaningful quantities, i.e., the number and energy density of the photons. Thus, we expect that since the peak distortions in a low $\Omega_B h^2$ universe at z_K occur at a low frequency, significant evolution of the temperature distortions can occur despite the relative inefficiency of bremsstrahlung. An examination of Fig. 4 supports these conclusions. The same initial spectrum $\delta n_\gamma/n_\gamma = 1.2 \times 10^{-2}$, $\delta\epsilon/\epsilon = 2.7 \times 10^{-2}$ is evolved in an (A) $\Omega_B h^2 = 2.5 \times 10^{-3}$ and (B) $\Omega_B h^2 = 0.10$ universe. Dashed lines represent the predictions of Eq. (42) with $x_\mu = x_c(z_K)$. In the low baryon density universe, the distortion peaks at low frequencies and represents a comparatively small physical distortion. Thus during the epoch $z_{\text{rec}} < z < z_K$, bremsstrahlung can significantly reduce low-frequency distortions and move the frequency of the peak upwards. For A, $x_{\text{peak}} = 8.3 \times 10^{-3}$ whereas $2x_c(z_K) = 3.6 \times 10^{-3}$. The high $\Omega_B h^2$ evolution, on the other hand, resembles the case of $\Omega_B h^2 = 0.025$ as in Fig.

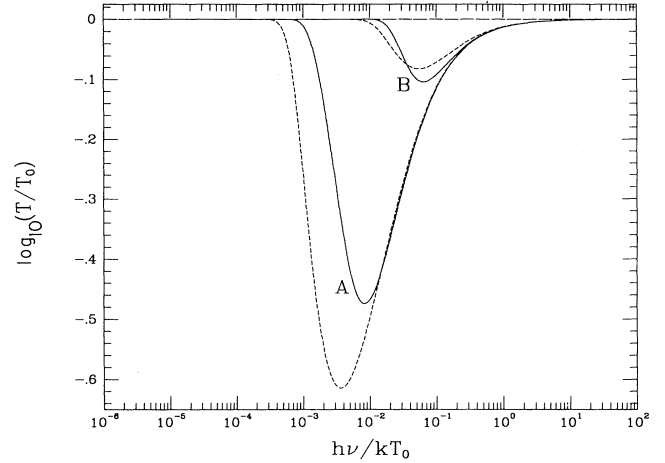


FIG. 4. Low-frequency dependence on $\Omega_B h^2$. Initial spectrum: injection with $\delta n_\gamma/n_\gamma = 1.2 \times 10^{-2}$, $\delta\epsilon/\epsilon = 2.7 \times 10^{-2}$ at $x_h = 6$, for $\Omega h^2 = 0.25$. (A) $\Omega_B h^2 = 0.0025$, $z_h = 1.2 \times 10^6$; (B) $\Omega_B h^2 = 0.10$, $z_h = 1.5 \times 10^5$. Dashed lines represent the analytic predictions for instantaneous freeze-out at $z = z_K$.

3. As elastic Compton scattering begins to freeze out, high-frequency distortions cease to evolve, whereas low-frequency distortions are more sharply suppressed than predictions. The peak shifting effect is, however, far less dramatic than in the extremely low $\Omega_B h^2$ case. Here $x_{\text{peak}} = 6.4 \times 10^2$ and $2x_c(z_K) = 5.4 \times 10^2$. Notice that in the high baryon density universe the amplitude of the distortions is larger than predictions due to the ineffectiveness of elastic Compton scattering at moving photons. On the other hand, distortions in an extremely low $\Omega_B h^2$ universe are smaller than predictions due to subsequent evolution at $z < z_K$. In all cases, however, these considerations of peak shifting and the reduction of distortions is a small effect as compared with the dependence of x_c on $\Omega_B h^2$.

In summary, employing $x_\mu \simeq x_c(z_K)$, we will underestimate x_{peak} by a factor of order unity. In a universe with $\Omega_B h^2$ given by nucleosynthesis or larger, the amplitude of the fluctuations is also underestimated by a factor of order unity in $\log_{10}(T/T_0)$. For extremely small $\Omega_B h^2$, the distortions are overestimated. These fluctuations appear at such low frequencies that out of equilibrium evolution significantly reduces them in comparison with predictions.

It is also interesting to examine what role double Compton scattering plays in determining the low-frequency spectrum. Let us return to the case described for Fig. 4. In an $\Omega_B h^2 = 2.5 \times 10^{-3}$ universe, $x_{c,\text{br}}(z_K) = 1.38 \times 10^{-3}$ and $x_{c,\text{DC}}(z_K) = 1.19 \times 10^{-3}$. This yields $x_c = 1.8 \times 10^{-3}$, a higher value than that predicted by bremsstrahlung alone. Thus at redshifts near z_K , which is the crucial regime for determining the location of the peak, these processes are equally effective. Of course, the steep dependence of double Compton scattering on redshift makes it unimportant at z_{rec} for any reasonable value of $\Omega_B h^2$. Figures 5(a) and 5(b) show a spectrum $\delta n_\gamma/n_\gamma = 2.5 \times 10^{-3}$, $\delta\epsilon/\epsilon = 5.5 \times 10^{-3}$, for $\Omega h^2 = 0.25$ evolved with and without double Compton

scattering for $\Omega_B h^2 = 2.5 \times 10^{-3}$, 0.015 and $z_h = 1.2 \times 10^6$, 4×10^5 , respectively. As expected, in the low $\Omega_B h^2$ case double Compton scattering plays a role in shifting the peak of the distortion upwards in frequency. It also helps to reduce the distortions at low frequencies by supplying photons. However, bremsstrahlung still plays the dominant role in defining the amplitude. For the case of $\Omega_B h^2 = 0.015$, double Compton scattering does not shift the peak since $x_{c,br}(z_K) \gg x_{c,DC}(z_K)$ and contributes a very small amount to the reduction of low-frequency distortions. Thus for $\Omega_B h^2$ given by nucleosynthesis or larger, bremsstrahlung alone is essentially responsible for determining the low-frequency behavior.

For the case of small negative chemical potentials, a very similar analysis holds. Figure 6 displays the time evolution of a small negative chemical potential ($\delta n_\gamma/n_\gamma = 7.5 \times 10^{-3}$, $\delta\epsilon/\epsilon = 2.7 \times 10^{-3}$, $z_h = 4 \times 10^5$) for $\Omega h^2 = 0.25$, $\Omega_B h^2 = 0.025$. Labels are as in Fig. 2. In

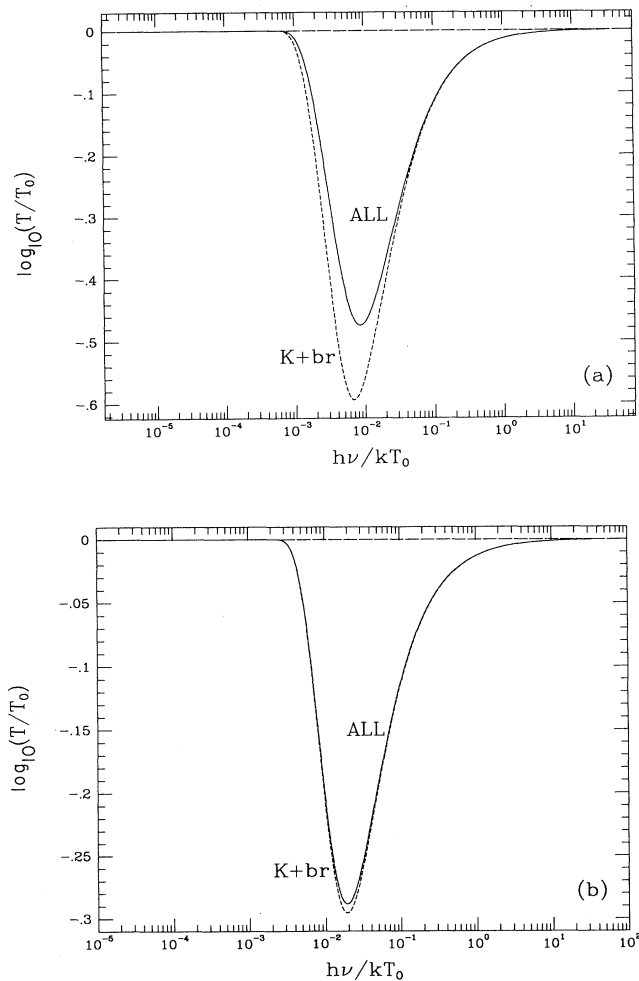


FIG. 5. Comparison of low-frequency spectrum with (solid) and without (without) double Compton scattering for (a) $\Omega_B h^2 = 0.0025$ and (b) $\Omega_B h^2 = 0.015$. Initial spectrum: injection at $x_h = 6$, with $\delta n_\gamma/n_\gamma = 2.5 \times 10^{-3}$, $\delta\epsilon/\epsilon = 5.5 \times 10^{-3}$ for $\Omega h^2 = 0.25$. Injection occurs at $z_h = 1.2 \times 10^6$ and 7×10^5 for (a) and (b), respectively.

Fig. 6(a), a δ -function injection of photons is thermalized under elastic Compton scattering, and a Bose-Einstein spectrum established. Here, an excess of photons is scattered downward by elastic Compton scattering until quasiequilibrium is established. It is essential to note that for small negative chemical potentials, number-changing processes are sufficiently effective at $x_e \simeq |\mu|$ to absorb the down scattered excess. Note also that the high-frequency spectrum fits well to a Bose-Einstein distribution of negative chemical potential and thus our qualitative analysis in Sec. III is verified. Furthermore, Eq. (37) also gives a reasonable approximation to the chemical potential in this case: $\mu = -9.8 \times 10^{-3}$, $\mu_{\text{pred}} = -1.0 \times 10^{-2}$.

Quasistatic evolution is shown in Fig. 6(b) and similar deviations from quasiequilibrium occur at $z \lesssim z_K$ as was the case for the positive chemical potential spectrum. During quasistatic evolution, a small negative chemical potential behaves very much like a small positive chemi-

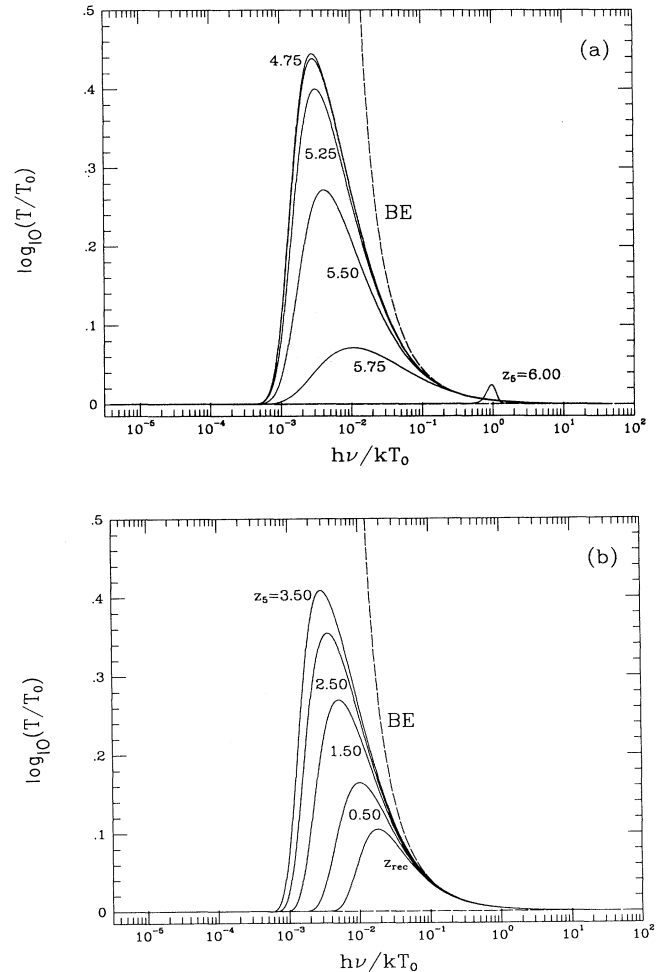


FIG. 6. Time evolution of low-frequency spectrum, $\mu < 0$. Initial spectrum: injection at $x_h = 1$, $z_h = 6 \times 10^5$ with $\delta n_\gamma/n_\gamma = 7.5 \times 10^{-3}$, $\delta\epsilon/\epsilon = 2.7 \times 10^{-3}$, for $\Omega h^2 = 0.25$, $\Omega_B h^2 = 0.025$. (a) Establishment of the Bose-Einstein spectrum $4.75 \times 10^5 < z < 6.00 \times 10^5$ where $z_{[5]} = z/10^5$. Unlabeled curve is $z = 5.00 \times 10^5$. (b) Quasistatic evolution and freeze-out $z_{\text{rec}} < z < 3.50 \times 10^5$.

cal potential and obeys the form given by Eq. (42). After z_K , bremsstrahlung and double Compton scattering no longer have to compete with elastic Compton scattering and sharply reduce the low-frequency distortions leaving the high-frequency spectrum untouched. Again, the evolution of the spectrum between z_K and z_{rec} moves the peak of the distortion slightly upward in frequency.

Figure 7 displays a typical fully evolved spectrum for an initial injection of $\delta n_\gamma/n_\gamma = 7.4 \times 10^{-2}$, $\delta\epsilon/\epsilon = 5.5 \times 10^{-2}$, at $z_h = 4 \times 10^5$ in an $\Omega h^2 = 0.25$, $\Omega_B h^2 = 0.025$ universe. Dashed lines represent the prediction given by $x_\mu = x_c(z_K)$. Again the numerical result has a peak distortion at a slightly larger frequency $x_{\text{peak}} = 1.86 \times 10^{-2} > 2x_c(z_K) = 1.79 \times 10^{-2}$ than analytic predictions. Distortions at the peak are also larger than predictions due to the ineffectiveness of elastic Compton scattering. Furthermore, the low-frequency side is suppressed more than predictions due to the evolution of the spectrum under bremsstrahlung for $z_K < z$. Thus small negative chemical potentials behave entirely in the same way as small positive chemical potentials. Large negative chemical potentials as we shall see in Sec. VI are suppressed due to their instability. They are, in any case, ruled out by observations.

One exceptional case is worth considering. When Eq. (37) predicts $\mu \simeq 0$, a more careful analysis is necessary. For injection at the critical frequency, $x_h \simeq 3.6$, μ vanishes to first order in the perturbations. Second-order perturbations would require slightly different values for $\delta n_\gamma/n_\gamma$ and $\delta\epsilon/\epsilon$ in order for μ to vanish. More importantly, there is a difference between a $\mu \simeq 0$ case in which $\delta n_\gamma/n_\gamma$ and $\delta\epsilon/\epsilon$ are balanced so as to in effect cancel, and a case in which $\mu \simeq 0$ purely due to the intrinsic smallness of perturbations. Given sufficient time, the two will evolve toward the same final spectrum. However, the spectrum may not reach equilibrium by recombination since in the balanced case we can inject an arbitrarily

large amount of energy. Large distortions take longer to thermalize even under elastic Compton scattering. Specifically, the spectrum does not relax down to the final equilibrium configuration implied by Eq. (37) on a time scale τ_K . Instead, another type of quasiequilibrium spectrum is established which in turn relaxes toward the actual equilibrium at a slower rate. At injection, the electrons are heated as in the case of a positive chemical potential. Photons are then scattered up from low frequencies leaving a low-frequency deficit of photons. However, just as in the case of the negative chemical potential, there is also an excess of photons at high frequencies. In fact, there is exactly the number needed to fill in the deficit at low frequencies. An intermediate spectrum forms in which the high-frequency spectrum behaves like a Bose-Einstein distribution with negative chemical potential whereas the low-frequency spectrum mimics one of a positive chemical potential. Given sufficient time, the high-frequency excess will fill the low-frequency deficit. However, it is quite possible that elastic Compton scattering will freeze-out before this has occurred.

Figure 8 displays an example. A large injection, $\delta n_\gamma/n_\gamma = 0.16$, $\delta\epsilon/\epsilon = 0.22$, is introduced at $x_h = 3.7$ and $z_h = 2.5 \times 10^5$ in a universe with $\Omega h^2 = 0.25$, $\Omega_B h^2 = 0.015$. The small shift in the critical frequency is due to the finite width of our so-called “ δ -function” injection and second-order effects. The high-frequency spectrum fits well to $\mu = -2.89 \times 10^{-3}$ whereas the low-frequency spectrum can be fit to the positive chemical potential behavior of $C_1 = +1.13 \times 10^{-2}$, $x_\mu = 7.0 \times 10^{-3}$. Notice that in these cases a comparatively small distortion at high frequencies can give rise to a large distortion at low frequencies. Here the low-frequency spectrum behaves as if $\mu \simeq 10^{-2}$ which is almost an order of magnitude greater than the actual chemical potential at high frequencies.

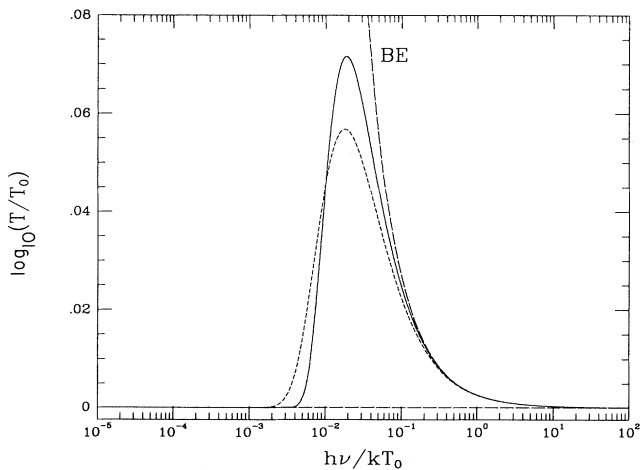


FIG. 7. Present day low-frequency spectra for $\mu < 0$. Initial spectrum: injection at $x_h = 2$, $z_h = 4 \times 10^5$ with $\delta n_\gamma/n_\gamma = 7.4 \times 10^{-3}$, $\delta\epsilon/\epsilon = 5.5 \times 10^{-3}$ for $\Omega h^2 = 0.25$, $\Omega_B h^2 = 0.025$. Dashed lines represent analytic prediction for instantaneous freeze-out at $z = z_K$.

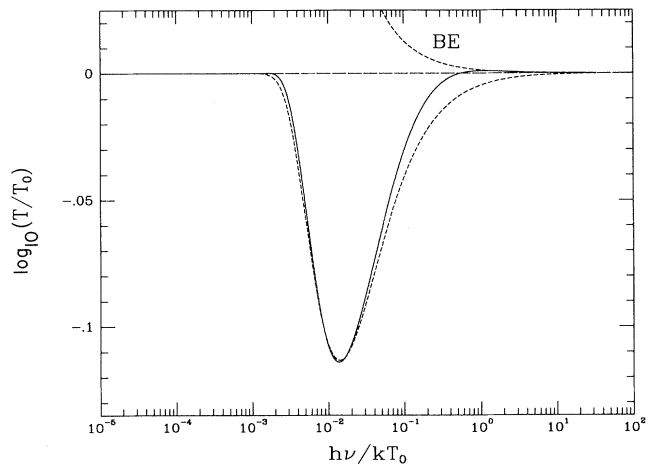


FIG. 8. Present day spectrum for exceptional case of $\mu_{\text{pred}} = 0$. Initial spectrum: injection at $x_h = 3.7$, $z_h = 2.5 \times 10^5$ with $\delta n_\gamma/n_\gamma = 0.16$, $\delta\epsilon/\epsilon = 0.22$ for $\Omega h^2 = 0.25$, $\Omega_B h^2 = 0.025$. Dashed lines are best analytic fit for high frequencies (Bose-Einstein with negative chemical potential) and low frequencies (exponentially suppressed positive chemical potential). See text for discussion.

If we inject this energy at an earlier time, we expect that distortions will be reduced by the mechanism described above. Figure 9 displays the dependence on z_h for the same initial spectrum described for Fig. 8. In order of decreasing distortions, the curves represent $z_h = 3.0 \times 10^5$, 4.0×10^5 , 5.0×10^5 , 6.0×10^5 , and 7.0×10^5 . The high-frequency regions can be fit to a Bose-Einstein spectrum of $\mu = -1.35 \times 10^{-3}$, -3.22×10^{-4} , -8.02×10^{-5} , -2.87×10^{-5} , and $\mu \approx 0$, respectively. For a redshift of $z_h = 7.0 \times 10^5$, the spectrum is fully thermalized under elastic Compton scattering, leaving essentially no distortions from blackbody.

Notice also that even these curious spectra retain the same position, again within a factor of order unity, for the critical frequency at which the peak distortions occur, $x_{\text{peak}} \approx 2x_\mu(z_K)$. This is because the analysis above for the location of the peak depends only on the balance between the number-changing processes and elastic Compton scattering. This balance, in turn, depends on $\Omega_B h^2$ alone. Thus the peak frequency is related to $\Omega_B h^2$ in the same manner for all three cases: positive, negative, and “zero” chemical potential. Equivalently, a measurement of the peak frequency yields information on the baryon density of the Universe.

Finally, for completeness, we should mention that solutions also exist for the opposite limit where $\mu'(x_e) \gg x_e > x_c$. We can extend the treatment of Illarionov and Sunyaev [16] to include double Compton scattering. In this regime, the spectrum must be rapidly changing with frequency, so that the kinetic equation reduces to

$$\frac{1}{x_e^2} \frac{d}{dx_e} \left[x_e^4 \frac{dn}{dx_e} \right] + \frac{t_K}{t_{\text{br}}} \frac{g(x_e)}{x_e^3} + \frac{t_K}{t_{\text{br}}} \frac{I_{\text{BE}}}{x_e^3} = 0 \quad (47)$$

for $x_e \ll 1$ and under the quasistatic conditions specified above, with the solution

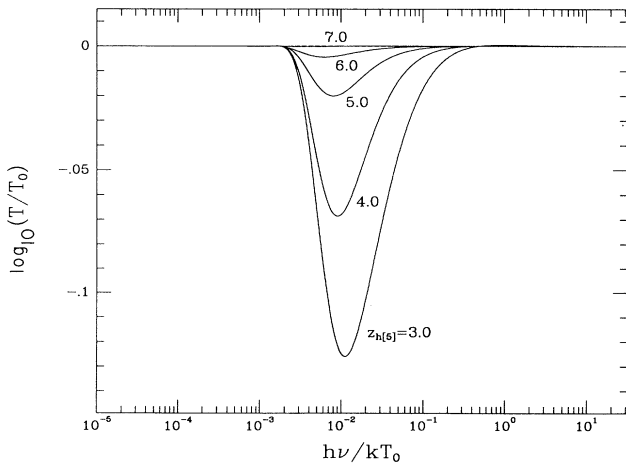


FIG. 9. Time evolution of an exceptional spectrum with $\mu_{\text{pred}} = 0$. Same spectrum and parameters as Fig. 8 for $z_h = 3.0 \times 10^5$, 4.0×10^5 , 5.0×10^5 , 6.0×10^5 , 7.0×10^5 in order of decreasing distortions. See discussion in text.

$$n(x_e) = \frac{2}{3} \frac{x_{c,\text{br}}^2}{x_e^3} \ln \frac{2.25}{x_{c,\text{br}}} \left[C_2 - \frac{\ln(2.25/x_e) - \frac{1}{3}}{\ln(2.25/x_{c,\text{br}})} \right] + \frac{4}{3} \frac{x_{c,\text{dc}}^2}{x_e^3} \ln(x_e). \quad (48)$$

However, the observational constraint on μ tells us that the *present* day spectrum will not have such a form, i.e., $\mu < 5 \times 10^{-3}$, so that $x_e \ll \mu'(x_e) < \mu$ cannot be satisfied simultaneously with $x_e > x_c$ for any reasonable choice of $\Omega_B h^2$. In any case, such frequencies would be far below the observational limit. However, such a form may be realized at higher redshifts when μ is not as tightly constrained.

VI. TIME EVOLUTION OF CHEMICAL POTENTIAL

In Sec. V, we have seen a special case in which the chemical potential can evolve purely under elastic Compton scattering. However, in the general case, the chemical potential only evolves if photons can be produced or absorbed. Furthermore, significant evolution of the high-frequency spectrum, $x_e \gg x_c$, can only occur at $z > z_K$ since elastic Compton scattering must be effective to redistribute these photons. Therefore, the approximations given in Sec. V for the form of the low-frequency spectrum are valid for these purposes. The low-frequency behavior governs the rate at which photons may be produced or adsorbed and thus is critical in determining the evolution of the chemical potential. If there is no energy release after the epoch of heating z_h , the rate of change of the chemical potential can be derived in a fashion similar to Eq. (37) for a static chemical potential. If we consider the number and energy density in the spectrum to be dominated by the high-frequency Bose-Einstein form, Eqs. (32) and (30) tell us

$$\begin{aligned} \frac{dn_{\gamma\text{BE}}}{dt} &= \frac{dn_{\gamma P}}{dT_e} \frac{dT_e}{dt} \phi(\mu) + n_{\gamma P} \frac{d\phi}{d\mu} \frac{d\mu}{dt}, \\ \frac{d\epsilon_{\text{BE}}}{dt} &= \frac{d\epsilon_P}{dT_e} \frac{dT_e}{dt} f(\mu) + \epsilon_P \frac{df}{d\mu} \frac{d\mu}{dt} = 0. \end{aligned} \quad (49)$$

We may solve these two equations simultaneously to obtain

$$\frac{d\mu}{dt} = - \left[\frac{4}{n_{\gamma\text{BE}}} \frac{dn_{\gamma\text{BE}}}{dt} \right] / B(\mu), \quad (50)$$

where

$$B(\mu) = 3 \frac{d \ln f(\mu)}{d\mu} - 4 \frac{d \ln \phi(\mu)}{d\mu}.$$

Equation (50) was first derived by Sunyaev and Zel'dovich [13]. The rate of change of the number density is given by integrating the kinetic equation (16):

$$\begin{aligned} \frac{1}{n_{\gamma\text{BE}}} \frac{dn_{\gamma\text{BE}}}{dt} &= \frac{1}{n_{\gamma\text{BE}}} \frac{8\pi}{c^3} \left[\frac{kT}{h} \right]^3 \int dx_e x_e^2 \frac{\partial n_{\text{BE}}}{\partial t} \\ &= \frac{1}{I_2 \phi(\mu)} \left[\frac{I_{\text{BE}}}{t_{\text{DC}}} J_{\text{DC}} + \frac{1}{t_{\text{br}}} J_{\text{br}} \right], \end{aligned} \quad (51)$$

where I_{BE} is defined in Eq. (34) and

$$J_{\text{DC}} = \int_0^{x_M} \frac{dx_e}{x_e} [1 - n(e^{x_e} - 1)] , \quad (52)$$

$$J_{\text{br}} = \int_0^\infty \frac{dx_e}{x_e} g(x_e) e^{-x_e} [1 - n(e^{x_e} - 1)] .$$

We have introduced a cutoff $x_M \simeq 1$ in the integration for the double Compton scattering source term since the kinetic equation (13) is not valid for high frequencies. However, since double Compton scattering is extremely inefficient at high frequencies, we expect that the error involved in truncating the integral is negligible.

As we can see from Eq. (52), the change in the number of photons depends on the integral of the low-frequency spectrum. From Sec. V, Eq. (42), we employ

$$n(x_e, t) = \frac{1}{\exp[x_e + \mu(t)\exp(-2x_e/x_e)] - 1} , \quad (53)$$

which is valid for small chemical potential, $\mu(t) < x_e$. In the limit that only double Compton scattering is effective, we obtain

$$\frac{d\mu}{dt} = - \frac{\mu}{t_{\mu, \text{DC}}(z)} \quad (54)$$

by employing Eq. (50). Here,

$$t_{\mu, \text{DC}}(z) = \frac{1}{4} B I_2 \left[\frac{t_K t_{\text{DC}}}{I_p} \right]^{1/2} \text{ s} ,$$

$$= 2.09 \times 10^{33} (1 - Y_p/2)^{-1} (\Omega_B h^2)^{-1} \times \Theta_{2.7}^{-3/2} z^{-9/2} \text{ s} . \quad (55)$$

The solution at the present time is

$$\mu(z=0) = \mu(z_h) \exp[-(z_h/z_{\mu, \text{DC}})^{5/2}] , \quad (56)$$

with

$$z_{\mu, \text{DC}} = 4.09 \times 10^5 (1 - Y_p/2)^{-2/5} \Theta_{2.7}^{1/5} (\Omega_B h^2)^{-2/5} . \quad (57)$$

This solution was first obtained by Danese and De Zotti [4].

For the case that bremsstrahlung dominates, a very similar equation holds:

$$\frac{d\mu}{dt} = - \frac{\mu}{t_{\mu, \text{br}}(z)} , \quad (58)$$

where

$$t_{\mu, \text{br}}(z) = \frac{1}{2} B I_2 \frac{t_{\text{br}}^{x_{c, \text{br}}}}{g(x_{c, \text{br}})} \simeq 3.4 \times 10^{25} (1 - Y_p/2)^{-1} (\Omega_B h^2)^{-3/2} \times \Theta_{2.7}^{5/4} z^{-13/4} \text{ s} , \quad (59)$$

where we have approximated $g(x_{c, \text{br}}) \simeq 5.4$. These equations yield the solution

$$\mu(z=0) = \mu(z_h) \exp[-(z_h/z_{\mu, \text{br}})^{5/4}] , \quad (60)$$

and

$$z_{\mu, \text{br}} \simeq 5.6 \times 10^4 (1 - Y_p/2)^{-4/5} (\Omega_B h^2)^{-6/5} \Theta_{2.7}^{13/5} . \quad (61)$$

Let us call the smaller of these two redshifts z_μ . The characteristic redshifts for double Compton scattering and bremsstrahlung are equal for a universe with

$$(\Omega_B h^2)_{\text{DC, br}} \simeq 0.084 (1 - Y_p/2)^{-1/2} \Theta_{2.7}^3 . \quad (62)$$

For a universe with a higher baryon density, bremsstrahlung should dominate the evolution of the chemical potential.

Note that these solutions are only valid in the case $\mu(z) < x_c(z) \ll 1$, for all z [25]. In many cases, $\mu(z) < x_c(z)$ during some but not all epochs of interest $z < z_h$. Furthermore, a small chemical potential today could have originated from a large distortion $\mu \gtrsim 1$ at high redshifts. Thus we must examine the behavior numerically and look for deviations from the forms of Eqs. (56) and (60).

Let us now examine the evolution of the chemical potential in a low $\Omega_B h^2$ universe as implied by nucleosynthesis. Numerical solutions suggest that Eq. (56) is indeed a good approximation for sufficiently small chemical potentials. Figure 10(a) shows such a case (the solid line is the numerical result, the dotted line is the best fit) for an initial spectrum $\mu(z_h) = 3.15 \times 10^{-3}$ with $\Omega h^2 = 0.25$, $\Omega_B h^2 = 0.025$. For comparison, $z_{\mu, \text{pred}} = 1.9 \times 10^6$ whereas $z_{\mu, \text{fit}} = 2.0 \times 10^6$. For very low redshifts, the distortion has not completely thermalized, even with respect to elastic Compton scattering, and thus the apparent chemical potential deviates from the expectations of Eq. (37). There has been insufficient time to scatter photons upwards in frequency to establish a perfect Bose-Einstein spectrum. The result is a spectrum that is very near Bose-Einstein in form but with a higher effective chemical potential at high frequencies.

Figure 10(b) shows a case with an intermediate chemical potential $\mu(z_h) = 1.84 \times 10^{-2}$ for $\Omega h^2 = 0.25$, $\Omega_B h^2 = 0.025$. We see that Eq. (56) still describes the evolution adequately but not entirely. The best-fit value of the critical redshift has shifted upwards, however, $z_{\mu, \text{fit}} = 2.2 \times 10^6$. This is because $\mu > x_c(z)$ for a significant portion of the evolution and the spectrum evolves more slowly than the exponential suppression given in Eq. (56) suggests. An examination of the low redshift behavior of Fig. 10(b) supports this assertion. Consequently, the effective critical redshift also increases. Comparing Figs. 10(a) and 10(b), we see that the evolution approaches the form of Eq. (56) and the predicted value for z_μ in the limit that the chemical potential is extremely small.

We can see this effect quite clearly for larger chemical potentials. Figure 11 shows such an evolution again for $\Omega h^2 = 0.25$, $\Omega_B h^2 = 0.025$. Curve *A* has an initial spectrum with $\mu(z_h) = 4.9 \times 10^{-1}$ curve *B*, $\mu(z_h) = 1.6 \times 10^{-1}$. Dashed lines represent the predictions of Eq. (56). For redshifts much less than z_μ , the chemical potential stays roughly constant, evolving more slowly than predictions. However, the fall off at high redshifts is correspondingly much more precipitous than Eq. (56) would imply. The effective redshift at which a substantial suppression of the

chemical potential occurs is increased but only by a factor of order unity. Attempts to fit the curves to the form of Eq. (56) yield $z_{\mu, \text{fit}} = 3.5 \times 10^6$, 3.0×10^6 for *A* and *B*, respectively. Note that in these cases, unlike Fig. 10(b), the form of Eq. (56), even leaving z_μ arbitrary, does not accurately trace the evolution. In general, then, a large positive chemical potential will exhibit stability up to a redshift $z \approx z_\mu$ and then fall dramatically.

For the case of small negative chemical potentials, we also expect that the redshift z_μ will play a critical role. Above this redshift, double Compton scattering has enough time to significantly evolve the high-frequency spectrum. Furthermore, for negative chemical potentials, the spectrum can only establish such a quasistatic equilibrium as required for this analysis if $|\mu| < x_{\text{exp}}(z_\mu)$. For larger negative chemical potentials and $z > z_\mu$, double Compton scattering is sufficiently effective to absorb this excess in photons and return the distribution to $|\mu| \approx x_{\text{exp}}(z_\mu)$. Thus *regardless of initial input of photons*

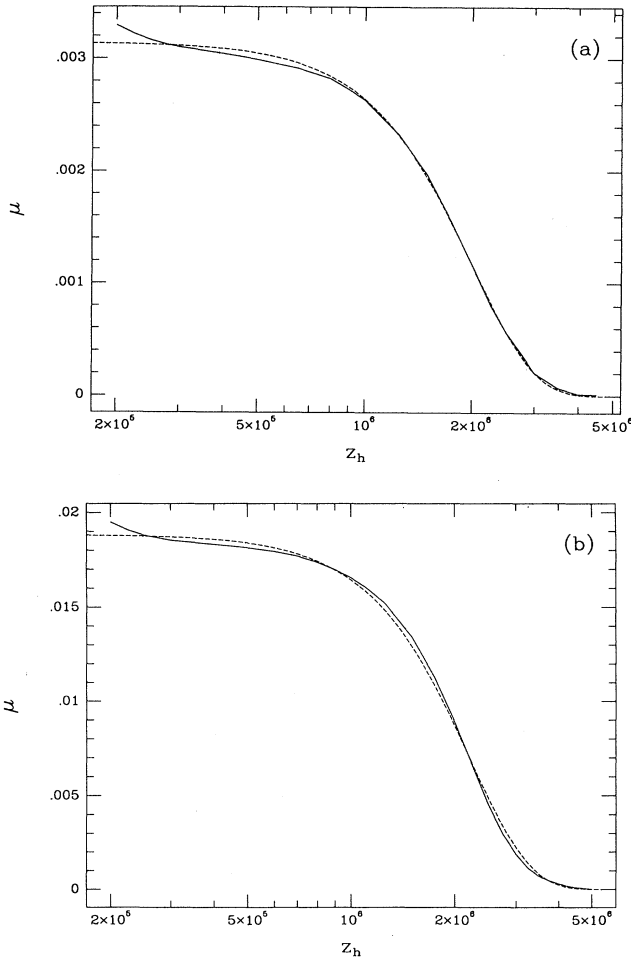


FIG. 10. Time evolution of small positive chemical potentials. (a) Small μ . Initial spectrum: injection of $\delta n_\gamma/n_\gamma = 2.5 \times 10^{-3}$, $\delta\epsilon/\epsilon = 5.5 \times 10^{-3}$. (b) Intermediate μ . Initial spectrum: injection of $\delta n_\gamma/n_\gamma = 5.4 \times 10^{-3}$, $\delta\epsilon/\epsilon = 2.0 \times 10^{-2}$. Both injections at $x_h = 6$ with $\Omega h^2 = 0.25$, $\Omega_B h^2 = 0.025$.

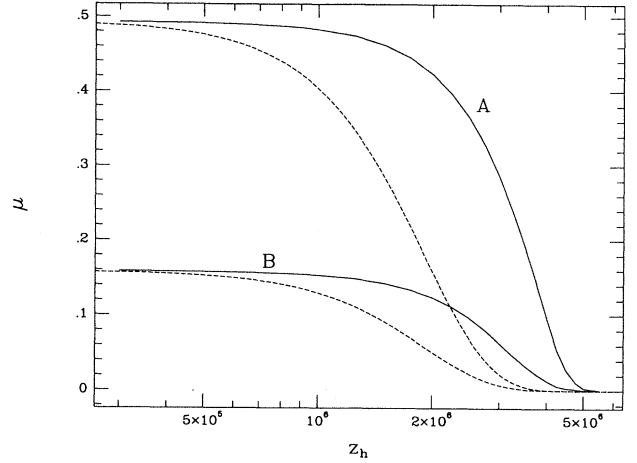


FIG. 11. Time evolution of large positive chemical potentials. (A) Extremely large μ . Initial spectrum: injection of $\delta n_\gamma/n_\gamma = 1.5 \times 10^{-1}$, $\delta\epsilon/\epsilon = 5.5 \times 10^{-1}$. (B) Large μ . Initial spectrum: injection of $\delta n_\gamma/n_\gamma = 4.4 \times 10^{-2}$, $\delta\epsilon/\epsilon = 1.6 \times 10^{-1}$. Both injections at $x_h = 6$ with $\Omega h^2 = 0.25$, $\Omega_B h^2 = 0.025$.

the evolution for $z > z_\mu$ will be approximately the same. Figure 12 displays this effect for $\Omega h^2 = 0.25$, $\Omega_B h^2 = 0.025$. Here, we inject successively larger numbers of photons and energies at the same frequency $x_h = 1$ (see figure captions for details). At high redshifts, we see that $\mu(z)$ saturates at some maximum value regardless of the initial input. For lower redshifts $z < z_\mu$, double Compton scattering is not sufficiently efficient. Elastic Compton scattering, as long as it is effective, will continue to scatter the excess down in frequency to be absorbed. Quasiequilibrium is never established and deviations from

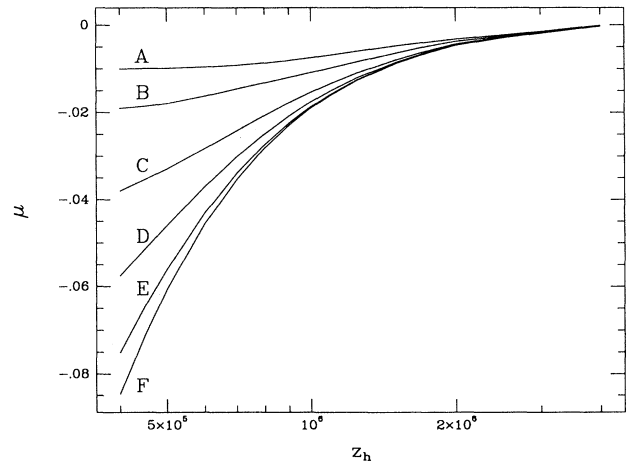


FIG. 12. Time evolution of negative chemical potentials. (A) $\delta n_\gamma/n_\gamma = 7.5 \times 10^{-3}$, $\delta\epsilon/\epsilon = 2.7 \times 10^{-3}$; (B) $\delta n_\gamma/n_\gamma = 1.5 \times 10^{-2}$, $\delta\epsilon/\epsilon = 5.5 \times 10^{-3}$; (C) $\delta n_\gamma/n_\gamma = 3.8 \times 10^{-2}$, $\delta\epsilon/\epsilon = 1.4 \times 10^{-2}$; (D) $\delta n_\gamma/n_\gamma = 7.5 \times 10^{-2}$, $\delta\epsilon/\epsilon = 2.7 \times 10^{-2}$; (E) $\delta n_\gamma/n_\gamma = 1.5 \times 10^{-1}$, $\delta\epsilon/\epsilon = 5.5 \times 10^{-2}$; (F) $\delta n_\gamma/n_\gamma = 3.0 \times 10^{-1}$, $\delta\epsilon/\epsilon = 1.1 \times 10^{-1}$. All for injection at $x_h = 1$ with $\Omega h^2 = 0.25$, $\Omega_B h^2 = 0.025$.

Eq. (56) are large. As can be seen in Fig. 12, large negative chemical potentials are rapidly evolved away under such a process. Small negative chemical potentials (A) exhibit the same stability as positive chemical potentials at redshifts $z < z_\mu$. Note also that this effect is only weakly dependent on $\Omega_B h^2$ (assuming double Compton scattering dominance):

$$x_{\text{exp,DC}}(z_\mu) \simeq 0.1(\Omega_B h^2)^{-1/10} \Theta_{2.7}^{-7/10}, \quad (63)$$

and so the critical chemical potential $\mu_c \simeq -x_{\text{exp}}(z_\mu)$ is roughly independent of both energy injection and $\Omega_B h^2$. Figure 13 (curves A and B) shows the evolution of the same initial spectra as Fig. 12 (curves E , F) for $\Omega_B h^2 = 0.10$. Notice that μ_c is roughly the same in both cases. Of course, we expect the estimate of the numerical constant above to be extremely crude, since z_μ itself is only an order of magnitude estimate of the epoch of effectiveness of double Compton scattering. Figures 12 and 13 show that the actual value is $\mu_c \simeq -0.02$ and is reasonably independent of $\Omega_B h^2$. Thus, elastic and double Compton scattering conspire to eliminate negative chemical potentials greater than a few percent. This result is approximately independent of the details of injection given reasonable choices of the cosmological parameters.

Now let us examine the effect of bremsstrahlung in a universe with high $\Omega_B h^2$. Figure 14 shows the evolution of a positive chemical potential with $\Omega_B h^2 = 0.10$ ($\delta n_\gamma/n_\gamma = 2.5 \times 10^{-3}$, $\delta\epsilon/\epsilon = 5.5 \times 10^{-2}$). Dotted lines show the evolution under double Compton scattering and bremsstrahlung individually, according to Eqs. (56) and (60). Notice that at redshifts $z < z_{\text{DC,br}} \simeq 6.7 \times 10^5$, bremsstrahlung dominates the evolution. Near $z \simeq z_{\text{DC,br}}$, double Compton scattering begins to dominate, evolving the spectrum rapidly with increasing redshift of heating. Note, however, that the combined influence can roughly be described as the sum of the contributions from the two processes considered individual-

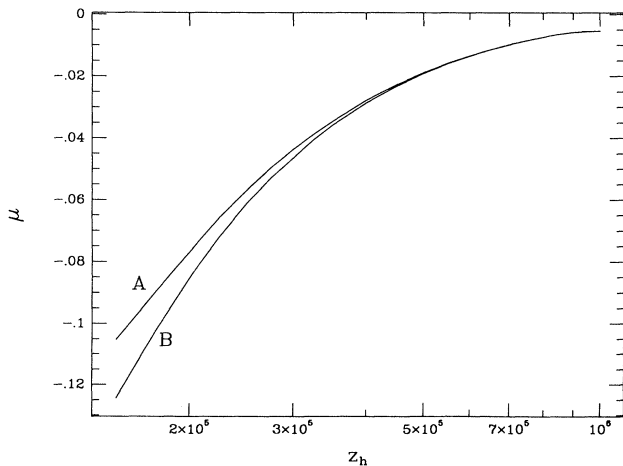


FIG. 13. High $\Omega_B h^2$ evolution of negative chemical potential. (A) $\delta n_\gamma/n_\gamma = 1.5 \times 10^{-1}$, $\delta\epsilon/\epsilon = 5.5 \times 10^{-2}$; (B) $\delta n_\gamma/n_\gamma = 3.0 \times 10^{-1}$, $\delta\epsilon/\epsilon = 1.1 \times 10^{-1}$, for injections at $x_h = 1$ with $\Omega h^2 = 0.25$, $\Omega_B h^2 = 0.10$.

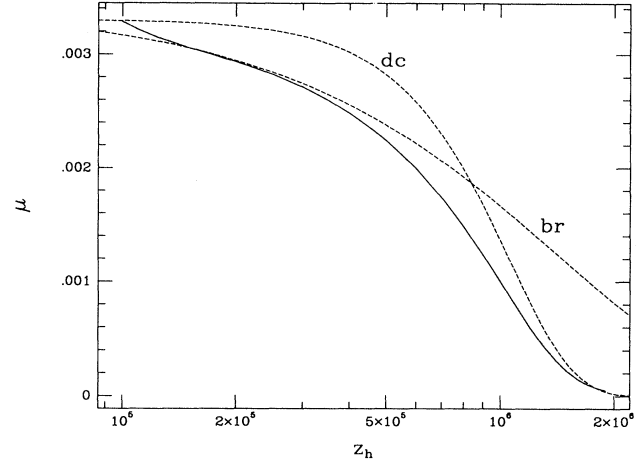


FIG. 14. High $\Omega_B h^2$ evolution of positive chemical potential, $\Omega h^2 = 0.25$, $\Omega_B h^2 = 0.10$. Initial spectrum: $x_h = 6$ with $\delta n_\gamma/n_\gamma = 2.5 \times 10^{-3}$, $\delta\epsilon/\epsilon = 5.5 \times 10^{-3}$. Dashed lines represent evolution expected when only double Compton scattering or bremsstrahlung is present.

ly, i.e., the interference between the processes is negligible. Thus, in a high $\Omega_B h^2$ universe, the evolution proceeds essentially as if bremsstrahlung alone were acting until $z_{\text{DC,br}}$ whereupon double Compton scattering and Eq. (56) play the crucial role.

In summary, Eqs. (56) and (60) describe the evolution adequately (in order of magnitude) within the range $-10^{-2} < \mu < 1$. The existence of a small positive chemical potential would place tight constraints on the energy injection mechanism. If the injection took place at $z_K < z < z_\mu$, the energy injected would have to be correspondingly small. Only if the injection took place in the narrow region, $z_\mu < z < \text{few} \times z_\mu$, would a large energy injection and a small chemical potential be consistent. Any earlier, and an arbitrarily large injection would be thermalized. On the other hand, the existence of a small negative chemical potential is not *a priori* as restrictive, since a large amount of energy can be injected and still lead to a small value for $|\mu|$. However, for an extremely small negative chemical potential, $\mu \simeq -3.3 \times 10^{-4}$ as required by observation, these considerations do not apply since we have determined numerically that the critical chemical potential for stability is $\mu \simeq -10^{-2}$. Extremely small negative chemical potentials are stable and equally as restrictive as small positive chemical potentials. The *nonexistence* of μ distortions of course would rule out nonstandard cosmologies with energy injection in the range $z_K < z < z_\mu$ but say very little about the physics for $z > z_\mu$. The one case that escapes these considerations is an injection where $\mu_{\text{pred}} = 0$ under Eq. (37). The chemical potential is driven to zero not by photon-creating processes but by elastic Compton scattering itself and thus z_μ is not the critical redshift for this process. Furthermore, an arbitrary amount of energy can be injected and still maintain a small chemical potential even at comparatively low redshifts. However, even this case is likely to leave a low-frequency signature which is potentially ob-

servable (Secs. V and VII). Thus the lack of low-frequency distortions would set tight bounds on all possible injections in this redshift range.

VII. COMPARISON WITH OBSERVATION

Recent results from FIRAS (Far Infrared Absolute Spectrophotometer) have placed tight constraints on the presence of a Bose-Einstein distortion in the Wien tail, $|\mu| < 3.3 \times 10^{-4}$ [1]. However, as we have shown in Sec. IV, the Rayleigh-Jeans regime is also interesting. It is there that we expect to see the largest temperature distortions, specifically at the frequency $x_{\text{peak}} \simeq 2x_c(z_K)$. For a positive chemical potential, the effective temperature of the Rayleigh-Jeans part of the spectrum is lower than that of the Wien tail. Figure 15 plots the observational results. Table I lists the actual points and the references in which the original data can be found. As is immediately obvious upon examination of Fig. 15, the average effective temperature of the cosmic background radiation in the Rayleigh-Jeans region is apparently lower than that of the Wien tail. Note that Fig. 15 is normalized so that T_0 is the temperature of the Wien tail, $T_0 = 2.726$ K [1]. We have also plotted the results of our numerical integration for comparison. This marginally significant distortion implies a quite large chemical potential in the Wien tail (dotted line, $\mu = 0.005$) that is inconsistent with the FIRAS results. If we were to require that the Wien distortions be consistent with FIRAS (solid line, $\mu = 3.3 \times 10^{-4}$), the predicted distortions in the Rayleigh-Jeans region would be far too small to explain the effect of the systematically low effective temperature.

Even so, distortions of this type may eventually be discovered, and it is therefore interesting to see what information can be gained from them. As described in Sec. IV, low-frequency behavior is governed by the balance

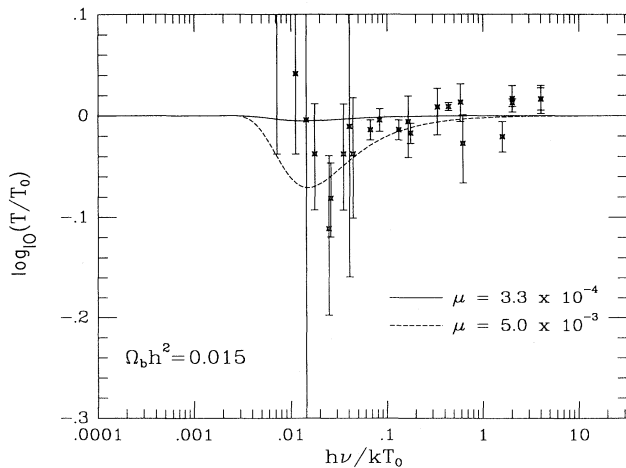


FIG. 15. Observational data given in Table I with numerical results for $\mu = 0.005$ (dotted) and $\mu = 3.3 \times 10^{-4}$ (solid line) with $\Omega_B h^2 = 0.015$ and $\Omega h^2 = 0.25$. The point $x = 0.007$, $\log_{10}(T/T_0) = 0.13$ falls beyond the limits of the graphs.

between bremsstrahlung and elastic Compton scattering, which is in turn sensitive to $\Omega_B h^2$ [see Eq. (24)]. At low frequencies, bremsstrahlung returns the spectrum to a Planck distribution. Thus, the critical frequency at which distortions peak is a *measure* of $\Omega_B h^2$. In light of recent attempts to avoid nucleosynthesis constraints and close the Universe with baryons [26], an independent constraint on $\Omega_B h^2$ is indeed desirable.

For illustrative purposes, Fig. 16 also displays the spectra obtained numerically for $\Omega_B h^2 = 0.0025, 0.015, 0.050, 0.25$, respectively, for a fixed Bose-Einstein Wien tail with $\mu = 3.3 \times 10^{-4}$. Note that the distortions are independent of the heating epoch, z_h and of the details of injection as long as the Wien tail is fixed in this manner (see below for the one exception). On the other hand, the location of the peak distortions is measurably different for various choices of $\Omega_B h^2$.

It is also interesting to consider the exceptional case in which both a large amount of energy is injected and Eq. (37) still predicts a small chemical potential. The distortions will typically freeze in before the spectrum has reached even the kinetic equilibrium configuration of $\mu = 0$ (see Sec. V). Particularly interesting is the fact that Rayleigh-Jeans distortions can be significant while Wien distortions remain minimal. Figure 17 displays examples with $\mu = -1.3 \times 10^{-3}, -3.2 \times 10^{-4}, -8.0 \times 10^{-5}$ in order of decreasing distortions. Note that the distortions on the low-frequency side are consistent with large deviations implied by the low effective temperature of the measurements to date even when high-frequency distortions are consistent with the already restrictive

TABLE I. Observational data for the effective temperature of the microwave background as a function of frequency $x = h\nu/kT_0$ where $T_0 = 2.726$ K.

x	T (K)	σ (K)	Ref.
0.007	3.7	1.2	[27]
0.011	3.0	0.5	[28]
0.014	2.7	1.6	[29]
0.018	2.5	0.3	[30]
0.025	2.11	0.38	[31]
0.026	2.26	0.19	[32]
0.035	2.5	0.3	[30]
0.040	2.66	0.77	[33]
0.044	2.79	0.15	[34]
0.044	2.50	0.34	[29]
0.067	2.64	0.07	[35]
0.083	2.70	0.07	[36]
0.132	2.64	0.06	[37]
0.165	2.69	+0.16/-0.21	[38]
0.175	2.62	0.06	[39]
0.333	2.78	+0.12/-0.17	[38]
0.435	2.783	0.025	[40]
0.579	2.81	0.12	[41]
0.614	2.56	+0.17/-0.22	[42]
1.579	2.60	0.09	[43]
2.000	2.796	+0.014/-0.039	[44]
2.000	2.807	0.025	[45]
4.002	2.83	0.09	[46]
4.002	2.832	0.072	[47]

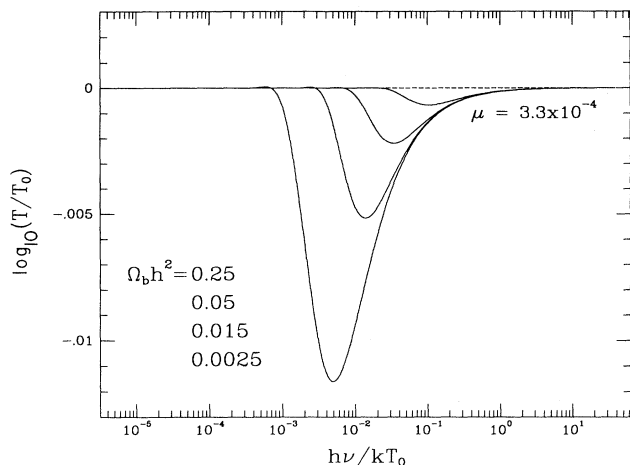


FIG. 16. Predicted spectral distortions with $\mu = 3.3 \times 10^{-4}$ for $\Omega_B h^2 = 0.0025, 0.015, 0.050, 0.25$ in order of decreasing distortions for $\Omega h^2 = 0.25$.

$|\mu| < 3.3 \times 10^{-4}$. We have expanded the scale for the graph as compared with Fig. 15 to bring out this effect. Alternatively, we can say that the injection of a large amount of energy even for this exceptional case in which high-frequency distortions vanish will lead to significant low-frequency distortions in many cases. Note also that the dependence of the peak distortion on $\Omega_B h^2$ is essentially unchanged. Thus, improved measurements in the Rayleigh-Jeans regime are desirable for a twofold purpose. If distortions are seen, they will give an interesting constraint on $\Omega_B h^2$ in all possible cases. If they are not seen, it will close the last loophole in the regime $z_{\text{rec}} < z < z_\mu$ for significant injection of energy.

VIII. CONCLUSIONS

We have presented analytical and numerical solutions of the Kompaneets equation with bremsstrahlung and double Compton scattering source terms, to study the instantaneous injection of photons in the early Universe prior to electron-proton recombination and after neutrino decoupling. The spectrum of the cosmic microwave background provides a unique probe of this era, in particular the redshift range $10^7 - 10^5$ when thermalization processes are becoming ineffective. Our predicted distortions are sensitive primarily to $\Omega_B h^2$, and will provide an important new measure of this fundamental parameter

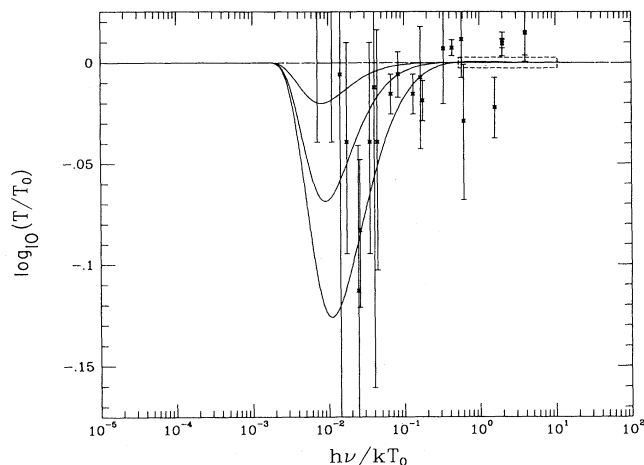


FIG. 17. Exceptional case of $\mu_{\text{pred}} = 0$ compared with observation. Wien tails of the plotted numerical results fit a negative chemical potential spectrum of $\mu = -1.3 \times 10^{-3}, -3.2 \times 10^{-4}, -8.0 \times 10^{-5}$ in order of decreasing distortion ($z_h = 3.0 \times 10^5, 4.0 \times 10^5, 5.0 \times 10^5$, respectively) and for $\Omega h^2 = 0.25, \Omega_B h^2 = 0.025, x_h = 3.7$. The points $x = 0.007, \log_{10}(T/T_0) = 0.13$ and $x = 0.11, \log_{10}(T/T_0) = 0.04$ fall beyond the limits of the graph. The boxed region denotes the typical domain of high-frequency measurements.

should chemical potential distortions be found. However, the marginal indications of distortions implied by low-frequency observations to date can only be explained by an exclusive class of energy injection scenarios that rely on symmetric injection about the blackbody peak. Furthermore, significant energy injection at $z \lesssim 5 \times 10^5 (\Omega_B h^2)^{-2/5}$ is ruled out in all but this one very restrictive scenario.

ACKNOWLEDGMENTS

We thank George Smoot for providing a compilation of the observational data on spectral distortions of the cosmic background radiation. One of us (W.H.) would like to thank Subir Sarkar and Douglas Scott for official suggestions and comments. After receiving the official COBE FIRAS report, Ref. [1], we were able to incorporate the new, more stringent constraints into the revised version of this paper. This research has been supported in part by grants from DOE and NSF.

- [1] J. C. Mather *et al.*, *Astrophys. J. Lett.* (to be published).
- [2] L. Danese and G. De Zotti, *Riv. Nuovo Cimento* **7**, 277 (1977).
- [3] A. P. Lightman, *Astrophys. J.* **244**, 392 (1981). Note that there is an omission of a factor of 4π in Lightman's expression for bremsstrahlung. This correction also applies for Refs. [7,20].
- [4] L. Danese and G. De Zotti, *Astron. Astrophys.* **107**, 39 (1982).
- [5] C. Burigana *et al.*, *Astron. Astrophys.* **246**, 49 (1991).

- [6] C. Burigana *et al.*, *Astrophys. J.* **379**, 1 (1991).
- [7] M. Fukugita and M. Kawasaki, *Astrophys. J.* **353**, 384 (1990). Their work should also be corrected by a factor of 4π for bremsstrahlung (see Ref. [3]).
- [8] S. Sarkar and A. M. Cooper, *Phys. Lett.* **148B**, 347 (1983).
- [9] A. S. Kompaneets, *Zh. Eksp. Teor. Fiz.* **31**, 876 (1957) [*Sov. Phys. JETP* **4**, 730 (1957)].
- [10] A careful treatment of the Kompaneets equation in the expanding Universe is given by R. Weymann, *Astrophys. J.* **145**, 560 (1966). For a particularly lucid derivation, see J.

- Bernstein and S. Dodelson, *Phys. Rev. D* **41**, 354 (1990).
- [11] J. Peyraud, *J. Phys.* **29**, 88 (1968).
- [12] Ya. B. Zel'dovich and E. V. Levich, *Pis'ma Zh. Eksp. Teor. Fiz.* **11**, 57 (1970) [*JETP Lett.* **11**, 35 (1970)].
- [13] R. A. Sunyaev and Ya. B. Zel'dovich, *Astrophys. Space Sci.* **7**, 20 (1970).
- [14] Ya. B. Zel'dovich and R. A. Sunyaev, *Astrophys. Space Sci.* **4**, 301 (1969).
- [15] K. L. Chan and B. J. T. Jones, *Astrophys. J.* **195**, 1 (1975).
- [16] A. F. Illarionov and R. A. Sunyaev, *Astron. Zh.* **51**, 698 (1974) [*Sov. Astron.* **18**, 413 (1975)].
- [17] A. F. Illarionov and R. A. Sunyaev, *Astron. Zh.* **51**, 1162 (1974) [*Sov. Astron.* **18**, 691 (1975)].
- [18] T. P. Walker *et al.*, *Astrophys. J.* **376**, 51 (1991); M. S. Smith, L. H. Kawano, and R. A. Malaney, *Astrophys. J. Suppl.* **85**, 219 (1993). We will not, however, constrain ourselves to choices of $\Omega_B h^2$ consistent with nucleosynthesis since we wish to test nonstandard scenarios, e.g., Ref. [28].
- [19] E. W. Larson *et al.*, *J. Comput. Phys.* **61**, 359 (1985).
- [20] J. Ellis *et al.*, *Nucl. Phys.* **B373**, 399 (1992). Their expressions for bremsstrahlung need to be corrected by a factor 4π (see Ref. [3]).
- [21] A. A. Zdziarski, *Astrophys. J.* **335**, 768 (1988).
- [22] Note that the case of an "induced decay" mentioned by K. Freese *et al.*, *Nucl. Phys.* **B287**, 797 (1987), and calculated by J. M. Overduin, P. S. Wesson, and S. Boyer, *Astrophys. J.* **404**, 1 (1993), in which the decay photons mimic the blackbody distribution of the background photons, does not satisfy this balance contrary to their assertion. The result of this type of decay is a spectrum with a negative chemical potential.
- [23] M. Ressel and M. Turner, *Comm. Astrophys.* **14**, 323 (1990).
- [24] A similar but more limited numerical study can be found in Refs. [5,6]. Our results are in excellent agreement with both their numerical work for the specific cases considered there and their analytic approximations.
- [25] Danese and De Zotti [4] also present solutions in the limit $1 \gg \mu(z) \gg x_c(z)$. However, this condition is hard to satisfy throughout the evolution due to the strong redshift dependence of x_c .
- [26] S. Dimopoulos *et al.*, *Astrophys. J.* **330**, 545 (1988). This method involves energy injection from particle decays and subsequent Klein-Nishina cascades. Hence it should be subject to the considerations here.
- [27] T. F. Howell and J. R. Shakeshaft, *Nature* **216**, 753 (1967).
- [28] K. S. Stankevich *et al.*, *Australian J. Phys.* **23**, 529 (1970).
- [29] G. Sironi *et al.*, *Astrophys. J.* **378**, 550 (1991).
- [30] S. A. Pelyushenko and K. S. Stankevich, *Astron. Zh.* **46**, 283 (1969) [*Sov. Astron.* **13**, 223 (1969)].
- [31] S. M. Levin *et al.*, *Astrophys. J.* **334**, 14 (1988).
- [32] M. Bensadoun *et al.*, *Astrophys. J.* **409**, 1 (1993).
- [33] T. Y. Otoshi and C. T. Stelzreid, *IEEE Trans. Instrum. Meas.* **24**, 174 (1975).
- [34] G. Sironi and G. Bonelli, *Astrophys. J.* **311**, 418 (1986).
- [35] G. De Amici *et al.*, *Astrophys. J.* **359**, 219 (1990).
- [36] N. Mandolesi *et al.*, *Astrophys. J.* **310**, 561 (1986).
- [37] S. M. Levin *et al.*, *Astrophys. J.* **396**, 3 (1992).
- [38] R. A. Stokes *et al.*, *Phys. Rev. Lett.* **19**, 1199 (1967).
- [39] S. Levin *et al.*, in *Particle Astrophysics: Forefront Experimental Issues*, edited by E. Norman (World Scientific, Singapore, 1989), p. 130.
- [40] D. G. Johnson and D. T. Wilkinson, *Astrophys. J. Lett.* **313**, L1 (1987).
- [41] G. De Amici *et al.*, *Astrophys. J.* **298**, 710 (1985).
- [42] D. T. Wilkinson, *Phys. Rev. Lett.* **19**, 1251 (1967).
- [43] M. Bersanelli *et al.*, *Astrophys. J.* **339**, 632 (1989).
- [44] P. Crane *et al.*, *Astrophys. J.* **346**, 136 (1989).
- [45] P. Palazzi *et al.*, *Astrophys. J.* **398**, 53 (1992).
- [46] D. M. Meyer *et al.*, *Astrophys. J. Lett.* **343**, L1 (1989).
- [47] P. Palazzi *et al.*, *Astrophys. J.* **357**, 14 (1990).